

Provided for non-commercial research and education use.  
Not for reproduction, distribution or commercial use.



This article appeared in a journal published by Elsevier. The attached copy is furnished to the author for internal non-commercial research and education use, including for instruction at the authors institution and sharing with colleagues.

Other uses, including reproduction and distribution, or selling or licensing copies, or posting to personal, institutional or third party websites are prohibited.

In most cases authors are permitted to post their version of the article (e.g. in Word or Tex form) to their personal website or institutional repository. Authors requiring further information regarding Elsevier's archiving and manuscript policies are encouraged to visit:

<http://www.elsevier.com/copyright>



Contents lists available at ScienceDirect

## Remote Sensing of Environment

journal homepage: [www.elsevier.com/locate/rse](http://www.elsevier.com/locate/rse)

## Monitoring land degradation risk using ASTER data: The non-evaporative fraction as an indicator of ecosystem function

Mónica García <sup>a,\*</sup>, Cecilio Oyonarte <sup>b</sup>, Luis Villagarcía <sup>c</sup>, Sergio Contreras <sup>d</sup>,  
Francisco Domingo <sup>a,e</sup>, Juan Puigdefábregas <sup>a</sup>

<sup>a</sup> Departamento de Desertificación y Geocología, Estación Experimental de Zonas Áridas (CSIC), Almería E-04001, Spain

<sup>b</sup> Departamento de Edafología y Química Agrícola, Universidad de Almería, Almería E-04120, Spain

<sup>c</sup> Departamento de Sistemas Físicos, Químicos y Naturales, Universidad Pablo de Olavide, Sevilla E-41013, Spain

<sup>d</sup> Grupo de Estudios Ambientales, Universidad Nacional de San Luis, San Luis E-5700, Argentina

<sup>e</sup> Departamento de Biología Vegetal y Ecología, Escuela Politécnica Superior, Universidad de Almería, Almería E-04120, Spain

### ARTICLE INFO

#### Article history:

Received 16 August 2007

Received in revised form 13 May 2008

Accepted 24 May 2008

#### Keyword:

Surface energy balance

Evapotranspiration

Eddy covariance

Desertification

Semiarid

Remote sensing

Disturbance

### ABSTRACT

There is a need to develop operational land degradation indicators for large regions to prevent losses of biological and economic productivity. Disturbance events press ecosystems beyond resilience and modify the associated hydrological and surface energy balance. Therefore, new indicators for water-limited ecosystems can be based on the partition of the surface energy into latent ( $\lambda E$ ) and sensible heat flux ( $H$ ).

In this study, a new methodology for monitoring land degradation risk for regional scale application is evaluated in a semiarid area of SE Spain. Input data include ASTER surface temperature and reflectance products, and other ancillary data. The methodology employs two land degradation indicators, one related to ecosystem water use derived from the non-evaporative fraction ( $NEF = H / (\lambda E + H)$ ), and another related to vegetation greenness derived from the NDVI. The surface energy modeling approach used to estimate the NEF showed errors within the range of similar studies ( $R^2 = 0.88$ ;  $RMSE = 0.18$  (22%)).

To create quantitative indicators suitable for regional analysis, the NEF and NDVI were standardized between two possible extremes of ecosystem status: extremely disturbed and undisturbed in each climatic region to define the NEFS (NEF Standardized) and NDVIS (NDVI Standardized). The procedure was successful, as it statistically identified ecosystem status extremes for both indicators without supervision. Evaluation of the indicators at disturbed and undisturbed (control) sites, and intermediate surface variables such as albedo or surface temperature, provided insights on the main surface energy status controls following disturbance events. These results suggest that ecosystem functional indicators, such as the NEFS, can provide information related to the surface water deficit, including the role of soil properties.

© 2008 Elsevier Inc. All rights reserved.

### 1. Introduction

Natural and human disturbances are known to modify the surface energy balance and hydrological cycle to different extents (Wang & Takahashi, 1998; Nicholson, 2000; Wilson et al., 2002; Liu et al., 2005), which may produce feedbacks to regional or even global climate patterns (Schlesinger et al., 1990; Xue & Shukla, 1993). Disturbance events pressing ecosystems beyond resilience cause land degradation (Puigdefábregas, 1995), defined as, "A reduction or loss in the biological and economic productivity and complexity of terrestrial ecosystems, as well as in the ecological, biochemical and hydrological processes that operate in them" (UNCCD, 1996).

Desertification is a process causing land degradation in arid, semiarid and dry-subhumid areas (hereinafter drylands) (UNCCD, 1996). At present, drylands cover more than 45% of the global land surface (Asner et al., 2003) and General Circulation Models (GCMs) predict increased aridity related to global warming (Okin, 2002). These areas sustain around 37% of the world's population (Reynolds et al., 2007) and are subject to climatic stress and strong pressures, which make them the regions most vulnerable to land degradation (Safriel et al., 2003). For these reasons, a better understanding of the relationships between disturbances, land degradation and water, the most limiting resource, is especially relevant in these regions.

There is currently a pressing need for operational, objective desertification indicators for large regions (Puigdefábregas & Mendizabal, 1998; Wessels et al., 2004; Reynolds et al., 2007). This lack of information is due in part to a change in the perception of desertification. It is now widely recognized that most of what was previously considered desertification was in fact response to climatic fluctuations (Prince

\* Corresponding author. Tel.: +34 950281045.

E-mail address: [monica@eeza.csic.es](mailto:monica@eeza.csic.es) (M. García).

et al., 1998; Tucker & Nicholson, 1999; Nicholson, 2000). The old “advancing desert” paradigm prevalent during the 1970’s and 1980’s is now obsolete and desertification is associated with a higher spatio-temporal heterogeneity of water and other resources with respect to undegraded areas (Schlesinger et al., 1990).

As several biophysical and biochemical processes are affected by desertification or land degradation in drylands, indicators of ecosystem status identify alterations in a wide range of properties, such as NPP (Net Primary Productivity), RUE (Rainfall Use Efficiency), soil properties (salinity, organic matter), vegetation patterns, landscape fragmentation, and water balance, among others (Schlesinger et al., 1990; Sharma, 1998; Asner et al., 2003), reflecting the complexity of the problem. Evapotranspiration is a key ecosystem function that has not been much used for desertification monitoring. In this regard, dysfunctional or degraded ecosystems are less capable of retaining, using and recycling local resources, such as water, energy and nutrients than ecosystems that are not (LeHouérou, 1996; Ludwig & Tongway, 2000; Paruelo et al., 2000; Holm et al., 2003; Boer & Puigdefábregas, 2003, 2005). As the partition of available energy reaching a surface into latent heat ( $\lambda E$ ) and sensible heat ( $H$ ) depends mostly on water availability, undegraded ecosystems should dissipate more energy through  $\lambda E$  (or evapotranspiration) compared to degraded or disturbed landscapes.

Therefore, development of regional-scale land degradation risk indicators evaluating alterations in the surface energy balance as a result of disturbances could be based on the energy partition between  $\lambda E$  and  $H$ . Remote sensing is the only data source currently providing frequent, spatially disaggregated information related to the surface energy status in the solar and thermal spectral ranges. Variables such as surface temperature, albedo or vegetation indices can be input into surface energy balance and evapotranspiration models (Kustas & Norman, 1996).

Results from research projects using remote sensing data and field methods, such as the SALSAs (Semi-Arid Land-Surface-Atmosphere) project in Arizona (Chehbouni et al., 2000), the HAPEX-Sahel (Hydrologic Atmospheric Pilot Experiment in the Sahel) (Goutorbe et al., 1997) or the EFEDA (European field experiment in a desertification threatened area) project in Spain (Bolle et al., 1993), have contributed to a better understanding the surface energy balance and evapotranspiration of drylands affected by land degradation. In a more applied context, land degradation has been assessed using thermal and reflectance data, either directly (Lambin & Ehrlich, 1997; Sobrino & Raissouni, 2000; Dall’Olmó & Karnieli, 2002; Mildrexler et al., 2007), or using remote sensing data as input to physical models (Wang & Takahashi, 1998). In general there is a trade-off between model parameterization requirements and applicability that has to be carefully considered.

The purpose of this study is to develop and test a new methodology to monitor land degradation risk by detecting disturbed sites for regional-scale application. The methodology consists of a water-use indicator related to ecosystem functioning (NEFS, Non-Evaporative Fraction Standardized), and another indicator related to vegetation greenness (NDVIS, Normalized Difference Vegetation Index Standardized). We hypothesize that disturbed sites, where land degradation might occur if the effect of disturbance is sustained over time, should show higher NEFs and lower NDVIS in response to increases in bare soil, and loss of vegetation and soil organic matter. Therefore, disturbed sites can be considered at risk of land degradation due to their loss of functionality. The changes in vegetation greenness and soil properties mentioned above should alter the surface energy balance by increasing the sensible heat flux ( $H$ ), and decreasing net radiation ( $R_n$ ) similar to other land degradation situations in North Africa (Dolman et al., 1997) and Southeast Spain (Arribas et al., 2003). However, feedback effects might modify some of these responses (Phillips, 1993) and depending on the magnitude of the changes in surface temperature and albedo, the partition of energy between sensible and latent heat flux may be quite different. Analysis of the NEFs, NDVIS and related variables at

disturbed and undisturbed sites will help to clarify some of these responses.

## 2. Study site and data

### 2.1. Study region

The study region (Fig. 1), located in the southeastern Iberian Peninsula (Almería, Spain), comprises 3600 km<sup>2</sup> (36.95°N, 2.58°W). It is characterized by its heterogeneity, with altitudinal gradients ranging from sea level up to 2800 m (a.s.l.) in the Sierra Nevada Mountains. Precipitation and temperature regimes vary widely due to the orography (López-Bermúdez et al., 2005). Annual precipitation is the lowest in the Tabernas lowlands, where it is less than 200 mm, while in the mountains it ranges from 400 mm to 700 mm, which is enough to sustain forest growth.

In the center of the study area, the karstic landscape of the Sierra de Gádor mountain range, covering 552 km<sup>2</sup>, consists of a series of thick carbonate rocks (limestones and dolomites), highly permeable and fractured with intercalated marl and less permeable calcschists underlain by impermeable metapelites (Aldaya et al., 1977). The southern edge of this mountain range is the main source of recharge for the Triassic aquifers in the region known as the “Campo de Dalías” (Pulido-Bosch et al., 2000). In general, the soils are very thin, rocky and vulnerable to flash flooding and erosion. The most common types vary depending on lithology and conservation status. On limestone and dolomitic materials, the most representative soils according to the Soil Taxonomy (Soil Survey Staff, 1990), are very thin Lythic Haploxeroll/Lythic Argixeroll (undisturbed sites) or Lythic Xerorthent (disturbed sites). The dominant types of less compact materials such as marls and calcschists are Typic Xerorthent and to a lesser degree Typic Haploxeroll (preserved sites) (Oyonarte et al., 1994).

The Sierra de Gádor Mountains underwent intense, widespread deforestation during the 18th and 19th centuries, when the original oaks (*Quercus ilex* L. and *Quercus faginea* Lam.), olive trees (*Olea europaea* L.), poplars (*Populus* L. spp.) and strawberry trees (*Arbutus unedo* Lam.) were cut down for ship construction and fuel for mining activities (Perez de Perceval, 1984). Current disturbances include construction, fire, agriculture and sheep grazing. At the present time, 73% of the Sierra de Gádor has a mixture with less than 50% vegetation cover comprised of sparse shrublands with rock outcrops, bare soil or grasses. The second largest natural land-cover type (12% of the area) is shrublands with a sparse cover of pine woodland (*Pinus* L. sp.), around 9% of the Sierra de Gádor is devoted to agriculture (mainly almond and olive trees) and only 1.5% of the land is covered by dense pine, reforested 30 years ago (Valle, 2003). The remaining 4.5% is composed of several different less representative land-use types (Contreras, 2006).

The rest of the study region, outside of the Sierra de Gádor, includes part of the Sierra Nevada Natural Park, which is comprised of pine forest with oak relicts and shrublands. There is an area of badlands, the Tabernas lowlands in the northeast, and along the ephemeral Andarax River there is a mosaic of citrus orchards and vineyards. One of the most salient features of the region is the more than 330 km<sup>2</sup> of plastic greenhouses in the “Campo de Dalías”. This unique combination of land covers and uses makes it a most interesting site for model testing. Within the study region three field sites were selected for validation purposes.

#### 2.1.1. Llano de los Juanes research site

Llano de los Juanes is a ~2 km<sup>2</sup> flat area with sparse shrubland, the same vegetation type present in 73% of Sierra de Gádor. It is located at an altitude of 1600 m in the high, well-developed karstic plain of the Sierra de Gádor. Vegetation cover is 50–60% and consists mainly of patchy perennial dwarf shrubs (30–35%) dominated by *Genista pumilla*, *Thymus serpyllodes* Bory, and *Hormathophylla spinosa* L., and grasses (20–25%) dominated by *Festuca scariosa* Lag. and *Brachypodium retusum* Pers. (Li et al., 2007).

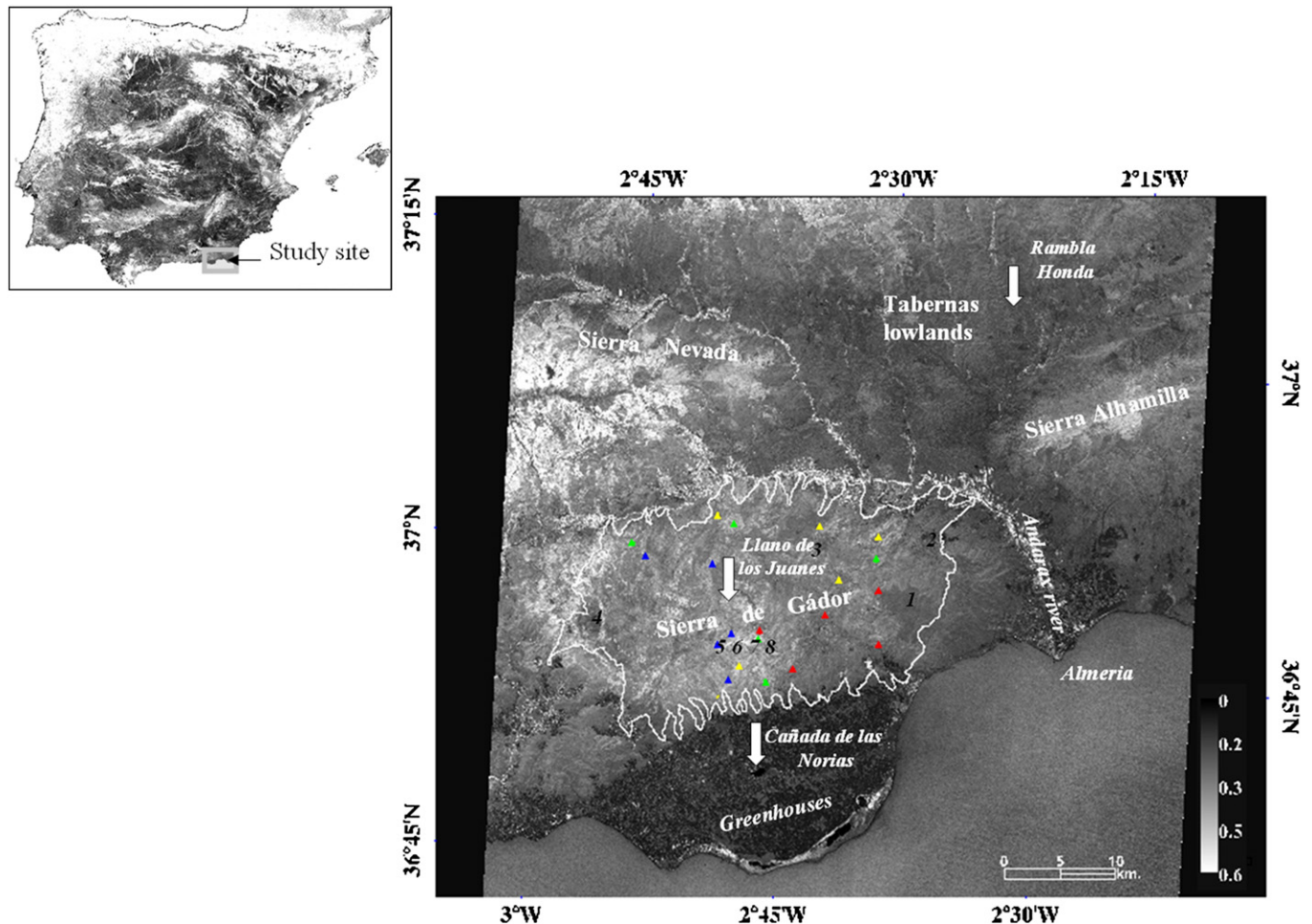


**Fig. 1.** Study site in Southeast Spain (Almería). The large image shows NDVI (15 m) from ASTER July,18-2004. Three mountain ranges, are visible, the Sierra Nevada, Sierra Alhamilla and Sierra de Gádor (outlined in white). The locations of the three NEF (Non-evaporative fraction) validation sites, Llano de los Juanes in Sierra de Gádor, Rambla Honda in the Tabernas lowlands, and the lake Cañada de las Norias by the greenhouse area are shown by white arrows. Validation sites of the land degradation indicator NEFS (NEF Standardized) included a set of severely disturbed sites and another set of disturbed-soil sites. Severely disturbed sites in Sierra de Gádor are identified as 1 (burnt scar), 2 (limestone quarry), 3 (almond orchards), 4 (abandoned mine). Undisturbed sites identified as 6 (dense oaks), 7 (oaks), 8 (sparse oaks), and 9 (old reforested pines). Disturbed -soil sampling sites on marl (red triangles), and limestone (yellow triangles) lithologies are shown, as well as control sampling sites on marls (green triangles), and limestones (blue triangles).

### 2.1.2. Rambla Honda research site

The Rambla Honda research site is located in a dry valley near Tabernas, Almería, Spain (37°8'N, 2°22'W, 630 m altitude). For a detailed description of the site, see Puigdefábregas et al. (1996). The valley has been abandoned for several decades and the activity is now restricted to small-scale sheepherding. Experiments related to hydrology and erosion (Puigdefábregas et al., 1999, 2005), surface energy balance and evapotranspiration (Villagarcía et al., 2007) and vegetation ecology (Hasse et al., 2000; Pugnaire et al., 1996) among others have been performed at the site during the last decade.

Three perennial species dominate the landscape, *Retama sphaerocarpa* (L.) Boiss shrubs on the valley floor, *Stipa tenacissima* L. tussocks on the steep sides of the valley and *Anthyllis cytisoides* L. shrubs on alluvial fans between the two. The valley floor has deep loamy soils overlying mica schist bedrock. The average annual rainfall is 220 mm with a dry season from June to September.

### 2.1.3. Cañada de las Norias wetland

The wetland, located in the greenhouse area, comprises 135 ha with a maximum depth of 2 m. The riparian vegetation is composed of *Phragmites australis*, *Tamarix canariensis*, and *Tamarix africana*, the latter also appears within the water table. Shallower parts are dominated by *Typha domingensis* and *Scirpus litoralis*. Within the wetland, macroalgae from

*Enteromorpha* and *Cladophora* genus, indicative of high eutrofication, tend to replace aquatic macrophytes (Paracuellos, 2006). Solids and algae increase water turbidity and reduce the effective penetration of solar radiation in the water column, which reduces the water storage term at a daily scale ( $G_d$ ) (Oswald and Rouse, 2004) that becomes almost negligible in the case of vegetated wetlands (Burba et al., 1999).

### 2.2. Micrometeorological data

Micrometeorological data have been acquired continuously at the Llano de los Juanes research site (Fig. 1) since September 2003. Latent and sensible heat fluxes were measured by an eddy covariance system using a three-dimensional sonic anemometer CSAT3 and a krypton hygrometer KH<sub>2</sub>O (both from Campbell Scientific Inc., Logan, USA). Fetch is sufficient for the vegetation height and sensors. Annual precipitation recorded during the last three hydrological years by a rain gauge installed in 2003 varied considerably: 506.7 mm in 2003/04, 212.4 mm in 2004/05, and 328.1 mm in 2005/06.

In Rambla Honda, there were no surface energy flux field measurements for 18-July-2004, the date of the ASTER scene covering this site. Therefore, daily sensible and latent heat fluxes for this site were simulated using a detailed SVAT (Soil-Vegetation-Atmosphere Transfer) multilayer evapotranspiration model for sparse vegetation (Domingo

et al., 1999). The model was parameterized for 18-July-2004 for the three dominant species at the site, *Retama sphaerocarpa*, *Anthyllis cytisoides*, and *Stipa tenacissima*. Model calibration was done previously using the Bowen Ratio Energy Balance (BREB) system for *Retama* and the same eddy covariance system later installed at Llano de los Juanes for *Anthyllis* and *Stipa*. RMSEs (relative to the mean in parenthesis) for the calibration for daily latent heat were  $8.28 \text{ Wm}^{-2}$  (6.48%),  $4.22 \text{ Wm}^{-2}$  (15.68%) and  $2.23 \text{ Wm}^{-2}$  (12.03%) for *Retama*, *Anthyllis* and *Stipa*, respectively. The % error of the mean for SVAT estimates of the three species together was 9.21% (Villagarcía et al., 2001).

Net radiation (NR-LITE; Kipp & Zonen, Delft, Netherlands), relative humidity (thermo hygrometer HMP 35C, Campbell Scientific, Logan, UT, USA), soil moisture (SBIB; Self Balance Impedance Bridge sensors) (Vidal, 1994; Domingo et al., 1999) and soil heat flux (HFT-3, REBS (Radiation Energy Balance Systems) Seattle, WA, USA) have also been continuously measured at Llano de los Juanes from September 2003 up to the present and in Rambla Honda from February 2002 to the present.

### 2.3. Remote sensing and spatial data

ASTER (Advanced Spaceborne Thermal Emission and Reflection Radiometer) data on July 9 and 18, 2004, and June 19, 2005 at 11.00 UTC were acquired for the study. ASTER, on board the Terra platform along with MODIS (Moderate Resolution Imaging Spectroradiometer), is currently the only sensor collecting multispectral thermal infrared data at high spatial resolution (French et al., 2005). The sensor scans a 60 km swath on the ground every 16 days with a swath angle of  $\pm 2.4^\circ$ . The sensor has nine reflective bands and five bands in the thermal infrared (TIR) region.

The ASTER products used in our research included surface reflectance (2AST07; HDFEOS version 2.8), with a spatial resolution of 15 m (VNIR) and 30 m (SWIR), and absolute accuracy of 4% of reflectance (Abrams & Hook, 2002). The kinetic temperature at 90 m (2AST08; HDFEOS version 2.8) represents a surface temperature absolute accuracy of 1–4 K (Abrams & Hook, 2002). No alerts regarding algorithm application have been reported in the quality assessment for the scenes. The three images did not cover exactly the same area because ASTER collects data at multiple off-nadir angles. For this reason, only one of the three scenes (July 18, 2004) covers the Rambla Honda field site. However, all three of them cover the Llano de los Juanes and the Cañada de las Norias lake field sites.

Images were acquired for the dry season (late spring and summer) because at this time, as evapotranspiration comes almost entirely from canopy transpiration, differences in NEF (Non-evaporative Fraction) between disturbed, less vegetated sites and undisturbed sites should be enhanced. Similarly, Mildrexler et al. (2007) have employed MODIS summer surface temperature to detect ecosystem disturbances. For southeast Spain, Arribas et al. (2003) have also identified summer as the season with the highest sensitivity to land degradation as represented in the Bowen ratio, surface temperature and climatic variables.

A digital elevation model (DEM) from the Regional Government of Andalusia (Junta de Andalucía) with 30 m resolution and a digital 0.5-m pixel orthophoto (from the Andalusian Regional Government) were used at different stages of the study.

Half-hourly air temperatures ( $^\circ\text{C}$ ) at the time of satellite overpass (11.00 UTC) were acquired from meteorological stations for validation purposes. Ten or eleven stations were available for each image depending on scene coverage. Seven of the stations belong to the EEZA (Estación Experimental de Zonas Áridas), and the rest to the Andalusian Regional Government (Red de Información Agroclimática de Andalucía).

We used a soil taxonomy map from Sierra de Gádor provided by Oyonarte (1992) and a soil water reserve map made using laboratory determinations of the water-holding capacity at 33 and 1500 kPa (field capacity and wilting point) in the fine-earth fraction of 80 representative profiles for the soil types described at Sierra de Gádor. Available

Water Content (AWC) in mm from each profile was estimated using the fine-earth fraction in soil volume and its apparent density down to contact with the bedrock. The spatial units in the final map are for soil associations. For each soil association an area-based weighted mean AWC was assigned from the AWC of the soil types in the spatial unit.

An aridity index map by Contreras (2006) calculated as the ratio between the long-term annual average potential evapotranspiration and precipitation was used. The average potential evapotranspiration was calculated with the Hargreaves–Samani equation (Hargreaves & Samani, 1982), previously calibrated with reference evapotranspiration measured at the study site agrometeorological stations. The Hargreaves & Samani (1982) equation is appropriate for semi-arid environments (Vanderlinden et al., 2004) and when meteorological information is scarce as it is within our study region.

### 3. Land degradation risk monitoring methodology

The rationale for the proposed methodology is based on the hypothesis that for a given climatic region, disturbed areas should have a lower vegetation greenness and a higher surface water deficit than undisturbed areas (Potter et al., 2003; Boer & Puigdefábregas, 2005; Mildrexler et al., 2007). Disturbed sites are considered “hot spots” at risk of land degradation due to their loss of functionality (Ludwig & Tongway, 2000) and because if the effects of the disturbance persist, land will become degraded. We detect disturbed sites in our work using snapshots. Nonetheless, periodic monitoring with snapshots can provide information about temporal trends and ecosystem resilience or degradation.

To assess land degradation risk by detecting disturbed sites, we propose two indicators derived from ASTER data, a functional land degradation indicator related to the surface water deficit (NEFS, Non-Evaporative Fraction Standardized), and another one related to vegetation greenness (NDVIS, Normalized Difference Vegetation Index Standardized).

Fig. 2 is a conceptual diagram showing the expected relationship between the two indicators. Undisturbed (control) sites should have a low NEFS (close to 0) and high NDVIS (close to 1). Disturbances should cause displacement in both indicators proportional to the disturbance

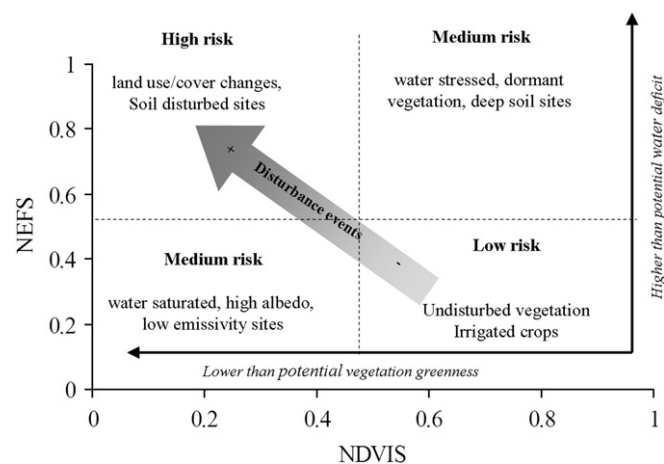


**Fig. 2.** Conceptual diagram showing the expected relationship between NDVIS (Normalized Difference Vegetation Index Standardized) and NEFS (Non-Evaporative Fraction Standardized) in a disturbance context. Undisturbed sites (lower left quadrant) correspond to NEFS close to 0 and NDVIS close to 1. Disturbance events should produce shifts in the indicators from potential status and disturbed sites are considered to be at risk of land degradation. To illustrate the land degradation risk concept four quadrants have been set: high risk of land degradation is considered with both NDVIS and NEFS significantly different from the control (undisturbed sites) and coinciding in diagnostic (across diagonal), medium risk when only one of the two indicators is significantly different from the control, and low risk when neither indicator is significantly different from the control.

strenght (i.e., along the diagonal, similarly to Nemani & Running (1997)) increasing NEFS and decreasing NDVIS accordingly. However, in some cases, only one indicator can be significantly different from the control while the other is not.

We consider the risk of land degradation to be higher the greater the magnitude of the differences in the indicators from undisturbed sites, and when both indicators coincide in the diagnostic (close to diagram diagonal). The chart has been divided into four quadrants, despite a continuum of values, to make it more understandable. High risk of land degradation is associated with NDVIS and NEFS significantly different from the control (undisturbed sites), medium risk when only one of the two indicators is significantly different from the control, and low risk when neither indicator is significantly different from the control.

In certain cases, the two indicators might provide opposite assessments. This can be attributed to a lack of convergence between structure and function at that particular time for a functional vegetation type (e.g. evergreen forest in summer) (Gamon et al., 1995) different from the functional type dominating in the undisturbed extreme of ecosystem status. NDVIS and NEFS might present opposite responses due to the many overlapping processes operating at different time and space scales within landscapes (Lambin, 1996) and the time scales that the proposed indicators are responding to are not always the same. Thus, evapotranspiration is conditioned by leaf area and canopy cover but is also closely coupled to atmospheric conditions and soil water content, and therefore is more dynamic than leaf area index (LAI) and canopy cover. For this reason, indicators related to vegetation greenness, such as the NDVIS, should be more stable, integrating past ecosystem processes to a greater extent and lagging behind indicators related to water deficit, such as the NEFS, which can be an early-warning indicator, but has to be more carefully evaluated in a temporal context.

Fig. 3 shows a flow chart with the main steps in the methodology used to monitor land degradation risk. First, the NEF (non-evaporative

fraction) was modeled from remote sensing and ancillary data and evaluated as a surrogate of the surface water deficit by comparing it with available field data. At this step, validation of NEF and surface energy fluxes was performed (i) quantitatively at three field sites (Llano de los Juanes, Rambla Honda and Cañada de las Norias) and (ii) qualitatively by evaluating NEF coherency using a set of different land cover types.

Because land degradation risk is a relative concept, in order to create meaningful quantitative indicators, boundary conditions for ecosystem status and climate type need to be established (Lambin & Ehrlich, 1997). This was done in a second step for both NDVI and NEF, yielding NDVIS (NDVI standardized) and NEFS (NEF standardized).

At this step, we evaluated the performance of the NEFS and NDVIS land degradation risk indicators at (i) severely disturbed sites where land use or land cover changes have occurred and (ii) at sites that have undergone soil surface horizon losses. Appropriate undisturbed sites in each case were used as controls (see locations in Fig. 1).

### 3.1. Estimating a water deficit indicator: the non-evaporative fraction (NEF)

In a previous study (García et al., 2007), three models requiring a simple parameterization for estimating the daily non-evaporative fraction ( $NEF_d$ ) were evaluated in Sierra de Gádor.

The MAE (Mean Absolute Error) of the regressions between  $NEF_d$  modeled and field data was 0.11 for the modified S-SEBI (Simplified Surface Energy Balance Index) model (Roerink et al., 2000), 0.14 for the so-called “simplified relationship” for unstable conditions (Seguin & Itier, 1983) and 0.18 for the approach of Carlson et al. (1995). However, due to the low size of the sample available for validation ( $n=9$ ), the 1:1 line was considered a better predictor of the goodness of fit for  $NEF_d$  values out of the range of the sample size, present in the images. For this reason, the simplified relationship was selected (slope=0.94; intercept=-0.08) instead of the modified S-SEBI (slope=0.75; intercept=0.18) or Carlson et al., 1995 (slope=0.70; intercept=0.01) estimates to calculate

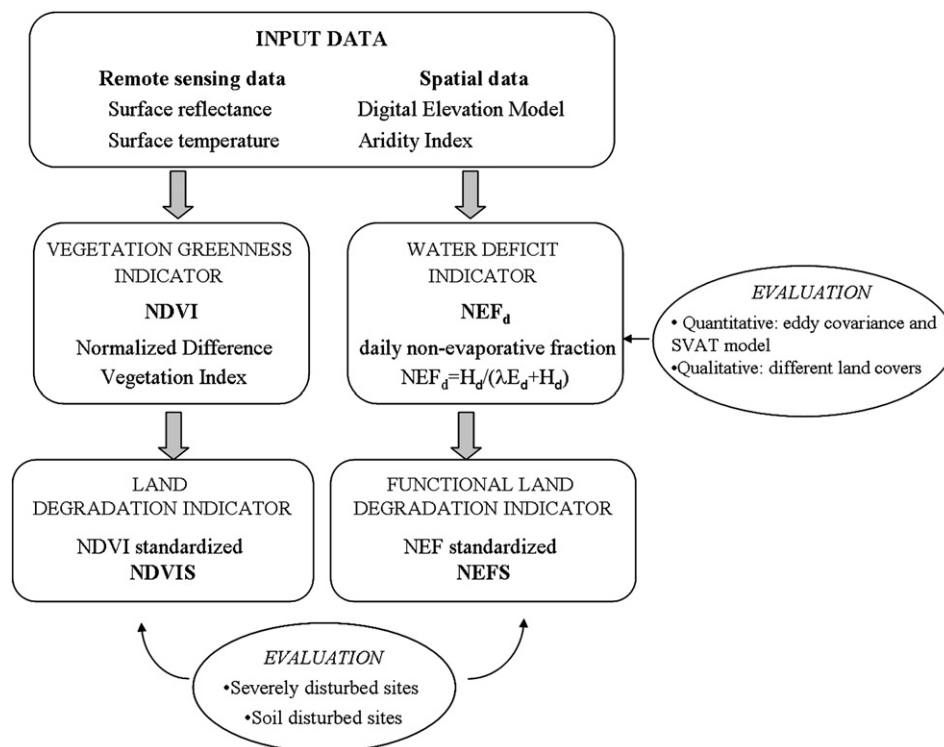


Fig. 3. Flow chart of the land degradation risk monitoring methodology proposed using two indicators, the NEFS (Non-Evaporative Fraction Standardized) related to water use and the NDVIS (Normalized Difference Vegetation Index Standardized) related to vegetation cover. These indicators were developed from the  $NEF_d$  (daily non-evaporative fraction) and the NDVI after rescaling between extremes for ecosystem status in each climatic region, enabling regional analysis. The methodology was first evaluated at an intermediate level to assess  $NEF_d$  reliability as a water deficit indicator, and finally NEFS and NDVIS were evaluated at disturbed and undisturbed sites as land degradation risk indicators.

daily NEF ( $NEF_d$ ) in this work.  $NEF_d$  was estimated from ASTER and ancillary data using the ratio between daily sensible heat ( $H_d$ ) derived from the “simplified relationship”, and daily net radiation ( $Rn_d$ ):  $H_d/Rn_d$ .

Daily soil heat flux ( $G_d$ ) can be considered negligible compared to the other components of the surface energy balance (Kustas & Norman, 1996; Seguin & Itier, 1983), as shown in Eq. (1)

$$NEF_d = 1 - EF_d = 1 - \frac{\lambda E_d}{\lambda E_d + H_d} = 1 - \frac{\lambda E_d}{Rn_d - G_d} = \frac{H_d}{Rn_d - G_d} \approx \frac{H_d}{Rn_d} \quad (1)$$

where  $EF_d$  is the daily evaporative fraction,  $\lambda E_d$  is daily latent heat flux ( $Wm^{-2}$ ),  $H_d$  is the daily sensible heat flux ( $Wm^{-2}$ ), and  $Rn_d$  is daily net radiation ( $Wm^{-2}$ ).

### 3.1.1. Daily net radiation ( $Rn_d$ )

Daily net radiation ( $Rn_d$ ) was calculated as the balance between incoming ( $\downarrow$ ) and outgoing fluxes ( $\uparrow$ ) of shortwave ( $R_s$ ) and longwave ( $R_l$ ) radiation. By agreement, incoming fluxes are positive and outgoing negative. Net radiation is the sum of net shortwave ( $Rn_s$ ) and net longwave radiation ( $Rn_l$ ) (Kustas & Norman, 1996).

First,  $Rn_i$ , instantaneous net radiation at the time of image acquisition, was calculated by estimating its four components, where the subscript  $i$  indicates instantaneous fluxes:

$$Rn_i = R_{s_i \uparrow} + R_{s_i \downarrow} + R_{l_i \uparrow} + R_{l_i \downarrow} = Rn_{s_i} + Rn_{l_i} \quad (Wm^{-2}) \quad (2)$$

The instantaneous shortwave net radiation ( $Rn_{s_i}$ ) was calculated using remote sensing data as in Eq. (3):

$$Rn_{s_i} = R_{s_i \downarrow} (1 - \alpha) \quad (Wm^{-2}) \quad (3)$$

$R_{s_i \downarrow}$  is the incoming solar radiation or incoming shortwave radiation, calculated at the time of the satellite overpass (11.00 UTC) using a solar radiation model (Fu & Rich, 2002) accounting for elevation, aspect, latitude and longitude, solar geometry, atmospheric transmissivity, and the influence of the surrounding topography.  $\alpha$  is the broadband surface albedo estimated according to Liang (2001) using six-band reflectance from ASTER Product 2AST07.

Longwave energy components are related to surface and atmospheric temperatures by the Stefan–Boltzmann Law. The instantaneous outgoing longwave radiation ( $R_{l_i \uparrow}$ ) was calculated at the time of image acquisition as in Eq. (4):

$$R_{l_i \uparrow} = -\varepsilon_s \sigma T_{s_i}^4 \quad (Wm^{-2}) \quad (4)$$

where  $\sigma$  is the Stefan–Boltzmann constant ( $5.67 \times 10^{-8} W m^{-2} K^{-4}$ ),  $T_{s_i}$  is surface temperature (K) at the time of satellite overpass, and  $\varepsilon_s$  is broadband emissivity for the surface, estimated based on the logarithmic relationship to NDVI as proposed by Vandegriend & Owe (1993). Radiometric surface temperature,  $T_{s_i}$ , was acquired directly from the ASTER kinetic temperature product (AST08) retrieved by the TES (Temperature Emissivity Separation) algorithm (Gillespie et al., 1998). An empirical function was used for the instantaneous incoming longwave radiation  $R_{l_i \downarrow}$  (Idso & Jackson, 1969). Daily net radiation ( $Rn_d$ ) ( $Wm^{-2}$ ) was calculated from  $Rn_i$  by assuming  $Rn_d/Rn_i \approx 0.3 \pm 0.03$  at summer midday as proposed by Seguin & Itier (1983).

### 3.1.2. Daily sensible heat flux ( $h_d$ )

The simplified relationship (Jackson et al., 1977, 1987; Seguin & Itier, 1983) states that  $\lambda E_d$  can be estimated from the difference between daily net radiation ( $Rn_d$ ) and daily sensible heat flux ( $H_d$ ), by estimating  $H_d$  from the difference between instantaneous surface ( $T_{s_i}$ ) and air temperatures ( $T_{a_i}$ ) near midday, as in Eq. (5):

$$H_d = B \cdot (T_{s_i} - T_{a_i}) \quad (mm \text{ day}^{-1}) \quad (5)$$

The simplified relationship has been verified empirically and theoretically (Seguin & Itier, 1983; Sugita & Brutsaert, 1991; Hall et al.,

1992; Kustas et al., 1994; Caselles et al., 1998).  $B$  can be understood as a mean exchange coefficient of sensible heat transfer. According to this relationship, the surface–atmosphere temperature gradient at midday, related to instantaneous sensible heat flux at midday by  $B$ , can be considered representative of the influence of  $H_d$  in the energy balance by assuming that the evaporative fraction is constant throughout the day (Seguin & Itier, 1983; Bastiaanssen et al., 1998a; Sugita & Brutsaert, 1991).

Seguin & Itier (1983) proposed two values for  $B$  as a first approximation,  $0.25 \text{ mm K}^{-1} \text{ day}^{-1}$  for stable atmospheric conditions ( $T_{s_i} - T_{a_i} < 0$ ) and  $0.18 \text{ mm K}^{-1} \text{ day}^{-1}$  for unstable conditions ( $T_{s_i} - T_{a_i} > 0$ ). At the time of image acquisition, unstable conditions tend to be prevalent in our study region (Domingo et al., 1999).

### 3.1.3. Air temperature ( $T_{a_i}$ )

Air temperature ( $T_{a_i}$ ) is used to estimate  $H_d$  and  $Rn_d$ . In order to develop an indicator that could be applicable to scarce-data sites, a methodology not requiring meteorological information was applied to estimate  $T_{a_i}$ .  $T_{a_i}$  was estimated from the images using the NDVI– $T_{s_i}$  triangle as proposed by Carlson et al. (1995) in an approach similar to Prihodko & Goward (1997) and Czajkowski et al. (2000). The apex of the NDVI– $T_{s_i}$  space (high NDVI and low temperature) should correspond to pixels with high NDVI located at the wet edge of the triangle that can be assumed to be at  $T_{a_i}$ .  $T_{s_i}$  at the apex was found by locating minimum surface temperature areas in the scene. Those with the highest NDVI, corresponding to forest patches, are identified, and the average  $T_{s_i}$  for that selected region is calculated.  $T_{a_i}$  was later corrected in order to include the impact of the strong altitudinal gradients present in the study area. A reference altitude, corresponding to the mean altitude for those pixels selected for the apex region, was computed as a baseline. Then positive corrections can be made for pixels below the baseline and vice-versa for pixels above it, at a lapse rate of  $6.5 \text{ }^\circ\text{C per } 1000 \text{ m}$ . This yields better results than considering a single  $T_{a_i}$  for the whole area by assuming constant meteorological conditions at the blending height as performed by Carlson et al. (1995).

### 3.2. Evaluation of the non-evaporative fraction ( $NEF_d$ ) as a water deficit indicator

Validation of surface energy fluxes estimated from remote sensing data is extremely complicated due to the limited availability of large-scale surface flux measurements for several surface types (Timmermans et al., 2007). In addition, field measurements and remote sensing footprints are not always comparable. In this paper we propose two validation procedures: (a) qualitative evaluation of the spatial consistency of  $NEF_d$  estimates from ASTER compared to  $NEF_d$  spatial averages from different land covers. (b) quantitative field validation: comparison between surface fluxes estimated using ASTER and measured at the field.

Table 1 explains procedure (b) showing the name of the site, the type of surface used for validation, the date when a field site was present in the ASTER image, the validation source used for comparison with model estimates for that field site, and finally, the variables validated in each case.

To compare the SVAT simulations for  $NEF_d$ ,  $H_d$  and  $Rn_d$  at Rambla Honda made with ASTER data, patches of the three plant species modeled were selected and ASTER estimates were spatially averaged within each patch. The patches ranged in size from 0.8 ha to 9.7 ha and were selected based on field visits and the aerial photo (0.5 m).

A lake, Cañada de las Norias, was also used for field validation type (b) for  $NEF_d$  and  $H_d$ . In this lake, a daily field value of  $H_d = 0$  was assumed, and so therefore,  $NEF_d = 0$  also, as in Bastiaanssen et al. (1998a) and Roerink et al. (2000). The  $NEF_d$  model used with ASTER data assumes  $G_d$  to be negligible compared with the rest of the components of the surface energy balance. This is acceptable for land (Seguin & Itier, 1983) but not for water surfaces. For this reason, ASTER model results for the lake were corrected for validation considering  $NEF_d = H_d / (Rn_d - G_d)$  instead of

**Table 1**

Sampling scheme for quantitative field validation of  $H_d$ ,  $NEF_d$  and  $Rn_d$  showing the name of the field site, the type of surface used for validation, the date in which the field site was present in each ASTER image (DATE), and the field validation source used in each case to be compared with model estimates

Field site name	Surface type	Date	Validation source	Fluxes validated
Llano	Shrubs	09-07-04	Eddy covariance	$H_d$ , $NEF_d$
Juanes			Net radiometer	$Rn_d$
Llano	Shrubs	18-07-04	Eddy covariance	$H_d$ , $NEF_d$
Juanes			Net radiometer	$Rn_d$
Llano	Shrubs	19-06-05	Eddy covariance	$H_d$ , $NEF_d$
Juanes			Net radiometer	$Rn_d$
Rambla Honda	<i>Retama sphaerocarpa</i>	18-07-04	SVAT (Domingo et al., 1999)	$H_d$ , $NEF_d$
Rambla Honda	<i>Anthyllis cytisoides</i>	18-07-04	SVAT (Domingo et al., 1999)	$H_d$ , $NEF_d$
Rambla Honda	<i>Stipa tenacissima</i>	18-07-04	SVAT (Domingo et al., 1999)	$H_d$ , $NEF_d$
Rambla Honda	Bare soil	18-07-04	Net radiometer	$Rn_d$
Cañada Norias	Lake	09-07-04	Assume $H_d=0$ ; $NEF_d=0$	$H_d$ , $NEF_d$
Cañada Norias	Lake	18-07-04	Assume $H_d=0$ ; $NEF_d=0$	$H_d$ , $NEF_d$
Cañada Norias	Lake	19-06-05	Assume $H_d=0$ ; $NEF_d=0$	$H_d$ , $NEF_d$

A SVAT (Soil–Vegetation–Atmosphere Transfer) multilayer model for sparse vegetation (Domingo et al., 1999) was used in Rambla Honda. At the lake  $H_d$  (daily sensible heat flux) and also  $NEF_d$  (non evaporative fraction) were assumed to be negligible. The last column shows the variables validated in each case.

$NEF_d = H_d / Rn_d$  by assuming a range of daily maximum and minimum  $G_d$  in the wetland of  $\pm 50 \text{ Wm}^{-2}$  ( $\pm 23\%$  of  $Rn_d$ ) (García et al., 2007).

Estimated spatial means of  $H_d$ ,  $Rn_d$  and  $NEF_d$  from each patch in the image and daily means from the field validation sources were compared using the variance of measurements and estimates, the correlation coefficient ( $R$ ), the RMSE (Root Mean Square Error), the MAE (Mean Absolute Error), and the probability ( $p$ ) of the regression.

### 3.3. Boundary conditions for ecosystem status and climate type

To create spatially comparable indicators suitable for regional analysis, the  $NEF_d$  and NDVI were standardized between two possible extremes of ecosystem status: extremely disturbed and undisturbed in each climatic region obtaining NEFS (NEF Standardized) and NDVIS (NDVI Standardized). We made the assumption that there was enough variability in the study region for there to be disturbed and undegraded or undisturbed areas. With this assumption, extremes for ecosystem status in each image can be found statistically with boundary-line analysis as the maximum and minimum of the particular variable for a given climate type (Boer & Puigdefábregas, 2005). The aridity index was used here as a climatic index.

The  $NEF_d$  for undisturbed areas should be at its lower boundary, as it is associated with the highest possible evapotranspiration level for local climate conditions. The NDVI for undisturbed areas should be at its upper boundary, associated with the highest possible vegetation greenness for those climatic conditions.

For each aridity index level,  $NEF_d$  and NDVI were standardized between 0 and 1 according to the maximum and minimum  $NEF_d$  or NDVI resulting in the NEFS and NDVIS. Boundary functions were found as the 5% and 95% quantile regression (Koenker & Hallock, 2001) between the  $NEF_d$  vs. the aridity index and the NDVI vs. the aridity index. Quantile regression, originally developed for econometric studies, is a statistical technique intended to estimate conditional quantile functions. Instead of estimating models for conditional mean functions as in classical regression, it allows to estimate models for any conditional quantile for a given population (Koenker & Hallock, 2001). In ecological studies, this type of analysis has proven very useful to detect relationships between two variables when other

factors not included in the model are known to affect the response of the dependent variable (Poyatos et al., 2005).

For each pixel, the standardized NEF (NEFS) was found as in Eq. (6):

$$NEFS = \frac{NEF_{d_{obs}} - NEF_{d_{5\%}}}{NEF_{d_{95\%}} - NEF_{d_{5\%}}} \quad (6)$$

where:

$NEF_{d_{obs}}$   $NEF_d$  observed in the pixel  
 $NEF_{d_{5\%}}$  lower  $NEF_d$  boundary  
 $NEF_{d_{95\%}}$  upper  $NEF_d$  boundary

The same procedure was followed to find the NDVIS (standardized NDVI).

### 3.4. Evaluation of land degradation risk indicators at disturbed sites

Mean differences in NDVIS and NEFS related to land degradation risk were evaluated using two sets of ground truth sites. The first set was from severely disturbed sites. The second dataset was from soil sites affected by soil degradation. Undisturbed sites were selected as controls in both cases.

#### 3.4.1. Severely disturbed sites: land use-land cover changes

In Sierra de Gádor, severely disturbed sites included areas where human activities have modified land use or recently burnt areas where land cover has changed very quickly. The impact of disturbances is observed as a loss of vegetation greenness and soil organic matter.

Selected disturbed sites included a burn scar from a severe fire in 2002, an active limestone quarry, an abandoned mining area, and almond orchards ploughed for weeds. Selection was based on field visits and aerial photointerpretation (0.5 m pixel). Undisturbed or control sites consisted of three different densities of oak woodlands (potential vegetation type), and an old reforested pine forest with a density cover close to the maximum expected for local climatic conditions (Valle, 2003) (Fig. 1). Evaluation of significant differences between sample means at disturbed and control sites was performed using two-tailed  $t$ -tests for independent samples implemented in the Statistica 7.1. software package (StatSoft, 2005).

#### 3.4.2. Disturbed soil sites

The second set of ground truth sites was related to more subtle, gradual changes. These processes, which might have occurred over long periods, are independent of current land use and not necessarily the result of recent changes. The *entisolization* index has been used to determine where historical soil degradation has occurred (Dazzi & Monteleone, 1998; Grossman, 1983). The entisolization concept is intended as an indicator of the impact of erosion on soils and is based on the fact that, as a result of erosion, deeper, more developed soil typologies tend to be replaced by poorly developed ones (Entisols). Areas dominated by Entisols are therefore characterized by a varying degree of soil losses due to current or past erosion processes (Ibañez et al., 2005; Grossman, 1983).

This qualitative index, created from soil taxonomy maps, was applied in the Sierra de Gádor mountains by Oyonarte et al., (2008), with soil degradation being associated with the disappearance of the mollic diagnostic soil horizon. The presence of a mollic horizon requires stable conditions at the surface favouring accumulation of soil organic matter, of at least 18-cm of horizon depth, and the organic fraction should be bound to the mineral fraction generating stable aggregates (Soil Survey Staff, 1990).

Table 2 shows the sampling design used to evaluate disturbed and undisturbed soil sites in Sierra de Gádor, stratified by the two dominant lithologic types (marls/calcschists and dolomitic/limestone; hereinafter referred to as marls and limestone, respectively) and by

**Table 2**  
Sampling scheme for degraded soil sites

Lithology	Soil type association	Disturbed
Dolomitic/limestone	Lithic Haploxeroll-Typic Calcixeroll	No
	Mollic Lithic Ruptic Xerothentic	Yes
	Xerochrept-Calcixerollic Xerochrept	No
Marls/calcsquists	Typic Haploxeroll-Mollic Xerochrept	No
	Typic Xerothent-Typic Xerochrept	Yes

Soils were classified as disturbed or undisturbed depending on the soil type association.

disturbance status. Selection of soil disturbed sites was blind to vegetation cover and just based on the soil type association having a mollic horizon present or not, according to the entisolization index.

To evaluate the land degradation risk indicators, five samples were taken for each of the four categories, limestone-disturbed, limestone-control, marl-disturbed, and marl-control. Each sample consisted of a 4×4 90-m pixel window (~13 ha/sample) and therefore, the number of selected pixels in each category was  $n = 16 \times 5 = 80$ . Each sample was taken in the centroid of a different soil polygon to account for spatial representativity and to avoid edge effects.

Variables analyzed were NEFS, NDVIS, NEF<sub>d</sub>, NDVI, as well as intermediate variables relevant for interpreting the results: albedo, surface temperature ( $T_{si}$ ), air temperature ( $T_{ai}$ ),  $T_{si} - T_{ai}$ , sensible heat ( $H_d$ ), net radiation ( $R_{nd}$ ) and instantaneous incoming shortwave radiation ( $R_{si\downarrow}$ ). As for severely disturbed sites, evaluation of significant differences between sample means at soil disturbed and control sites was performed using two-tailed *t*-tests for independent samples stratified by geological type and implemented in the Statistica 7.1. software package (StatSoft, 2005).

## 4. Results and discussion

### 4.1. Evaluation of the water deficit indicator: non-evaporative fraction (NEF)

The NEF<sub>d</sub> (daily non-evaporative fraction) and the main variables involved in its estimation, air temperature, daily sensible heat flux ( $H_d$ ), and daily net radiation ( $R_{nd}$ ) were evaluated.

#### 4.1.1. Air temperature

The overall fit of meteorological station and estimated data was MAE < 2.1 °C (Table 3), but  $T_{ai}$  estimates are subject to local errors. Altitude is not the only factor affecting  $T_{ai}$ , but using this approach has the advantage of not having to use meteorological station data and yields better results than considering a single  $T_{ai}$  for the whole area by assuming constant meteorological conditions at the blending height as performed by Carlson et al. (1995). Also, any systematic error in  $T_{si}$  retrieval will propagate in  $T_{ai}$ . These errors should therefore partially cancel when calculating  $T_{si} - T_{ai}$  differences in estimating  $H_d$ .

**Table 3**  
Air temperature validation at the study site

	18-07-2004	09-07-2004	19-06-2005
	N = 11	N = 10	N = 12
$R^2$ (observed-predicted)	0.61	0.74	0.67
MAE before adjustment (°C)	4.31	3.40	2.68
MAE after adjustment (°C)	1.96	2.07	1.93

MAE (Mean Absolute Error) before adjustment is the average absolute difference in residuals between estimated and measured air temperature at the meteorological stations. MAE after adjustment is the average absolute difference in residuals between estimated values that have been corrected for altitudinal effects and measured air temperature at the meteorological stations. n is the number of stations within each ASTER scene.

### 4.1.2. Daily net radiation ( $R_{nd}$ )

$R_{nd}$  estimates using ASTER data show a correspondence with field data (Table 4), with an RMSE of 9 Wm<sup>-2</sup> (<5% of  $R_{nd}$ ) similar to the reported  $R_{nd}$  accuracy of the net radiometer, around ±10% (NR-lite by Kipp & Zonen).

In the same conditions, Rn errors at daily scales should be lower than at instantaneous scales due to averaging (Bisht et al., 2005). However, depending on input data, model and surface type used, a wide range of errors can be found which together with different ways of error reporting, makes comparisons complicated among different studies. For instance, approaches combining sun-synchronous remotely sensed data with meteorological data obtained RMSEs between 20–45 Wm<sup>-2</sup> for hourly and half-hourly estimates (Su, 2002; Jacob et al., 2002; Gómez et al., 2005; Timmermans et al., 2007). At daily scales, Hurtado & Sobrino (2001) obtained an RMSE of 42.5 Wm<sup>-2</sup> combining meteorological information and NOAA-AVHRR data and Samani et al. (2007) using ASTER data, obtained standard errors of daily estimates between 13.2–61.8 Wm<sup>-2</sup>. Using exclusively remotely sensed information during one year (15 MODIS images), Bisht et al. (2005) obtained RMSEs of 74 Wm<sup>-2</sup> (15-minute estimates) and 61.8 Wm<sup>-2</sup> for daily estimates.

### 4.1.3. Daily sensible heat flux ( $H_d$ ) and the non-evaporative fraction (NEF<sub>d</sub>)

Qualitative evaluation showed coherent NEF<sub>d</sub> spatial patterns with those expected for these dates and land cover types (Fig. 4). Throughout the study region, the lowest NEF<sub>d</sub> was for water and high-altitude mountain forests. The highest NEF<sub>d</sub> values were found in the Tabernas lowlands (including the R. Honda research site) and abandoned mines in Sierra de Gádor, which is plausible at this time of the year.

Quantitative validation results were similar for NEF<sub>d</sub> and  $H_d$  (Wm<sup>-2</sup>) due to the low  $R_{nd}$  error (Tables 5 and 6). In addition to the oversimplification of the modeling approaches, error is propagated from input data. Thus, although reported errors in  $T_{si}$  are within acceptable quality levels (<4 K), they contribute to final error combined with the error in  $T_{ai}$  estimates (<2 K) and in the aerodynamic resistance. For instance at Llano de los Juanes  $H_d$  and NEF<sub>d</sub> underestimates are related to an overestimation in the aerodynamic resistance.

**Table 4**  
Quantitative field validation for daily net radiation  $R_{nd}$  (Wm<sup>-2</sup>) using *Retama*, *Anthyllis*, *Stipa*, shrubs, and bare soil sites

Date	Surface type	Location	Field	ASTER	AE (Wm <sup>-2</sup> )	% Error
			$R_{nd}$ (Wm <sup>-2</sup> )	$R_{nd}$ (Wm <sup>-2</sup> )		
09-07-04	Shrubs	Llano Juanes	188.70	184.21	4.49	1.30
18-07-04	Shrubs	Llano Juanes	179.71	189.70	9.99	5.30
19-06-05	Shrubs	Llano Juanes	183.40	192.40	9.00	4.90
18-07-04	<i>Retama</i>	Rambla Honda	166.53	152.53	14.00	-8.41
18-07-04	<i>Anthyllis</i>	Rambla Honda	165.07	156.59	8.48	-5.14
18-07-04	<i>Stipa</i>	Rambla Honda	159.28	155.97	3.31	-2.08
18-07-04	Bare soil	Rambla Honda	112.68	110.19	2.49	-2.21
Std			25.46	28.91		
MAE			7.39			
RMSE			8.94			
R			0.95			
p			0.0008			

The column "Field" indicates  $R_{nd}$  field estimates, and "ASTER" the  $R_{nd}$  estimated using ASTER and ancillary data. AE is the absolute difference between ( $R_{nd}$  field -  $R_{nd}$  ASTER). The % Error is calculated as ( $R_{nd}$  field -  $R_{nd}$  ASTER)100/ $R_{nd}$  field. Std is the standard deviation of Field and ASTER estimates. For overall error evaluation, the MAE (mean absolute error), average AE, R (Pearson correlation coefficient), and p (probability), between field and ASTER results were calculated.

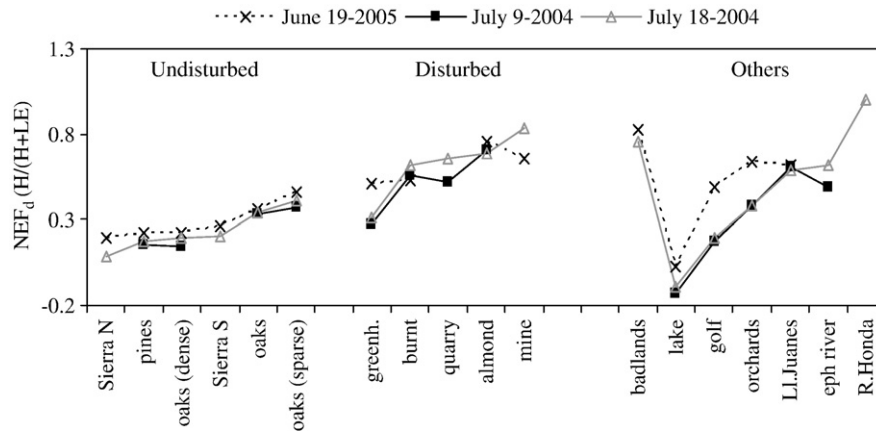


**Fig. 4.** Qualitative evaluation of  $NEF_d$  (daily non-evaporative fraction) on selected surface types estimated with ASTER on three days. The first set of surfaces corresponds to undisturbed sites. Sierra N and Sierra S are pine forests on the northern and southern slopes of the Sierra Nevada mountain range, while oaks (dense), oaks (sparse) and oaks are relict oak woodlands of varying densities in Sierra de Gádor. Pines correspond to old reforested sites, also in Sierra de Gádor. The second set is for disturbed sites: greenhouses (Greenh.), a strong burn scar (burnt), a limestone quarry (quarry), almond orchards (almond), and an abandoned mining area (mine). The third set is comprised of miscellaneous sites: the Tabernas lowlands, Cañada de las Norias wetlands (lake), a golf course (golf), irrigated citrus orchards along the Andarax river (orchards); L.L. Juanes is the Llano de los Juanes, eph. river is the ephemeral Andarax River and R.Honda is the Rambla Honda research site. The location of these sites can be seen in Fig. 1.

We should also be aware that the eddy covariance and Bowen Ratio Energy Balance techniques are subject to error. Uncertainty is around 20% in the eddy covariance system (Baldocchi et al., 2001) and 10% in the Bowen Ratio Energy Balance method (Nie et al., 1992; Gurney & Sewell, 1997). Moreover, in semiarid areas with sparse vegetation cover, the error in energy fluxes tends to be even higher, around 25% (Were et al., 2007). In addition, although the SVAT model error is estimated as less than 10%, within the uncertainty of the instrumental measurements, it was calibrated during a prior period that was considered representative enough of the variability found in surface and climate variables at longer time scales.

In general, the reported range of errors in  $H_d$  varies widely depending on surface type, image data, average time period, and model used, and it is generally also more complicated to get accurate estimates for heterogeneous semiarid areas than for agricultural or humid sites (Wassenaar et al., 2002).  $H_d$  estimates from remote sensing models usually contribute the highest uncertainty to the

surface energy balance. Typical errors are around 20–30% or 1 mm day<sup>-1</sup>, equivalent to ~29 Wm<sup>-2</sup> in  $H_d$  (Kustas & Norman, 1996). In our case, the RMSE for  $H_d$  is below that threshold with individual errors between 3% and 30% (Llano de los Juanes).

Seguin et al. (1999) consider an error of around 50 Wm<sup>-2</sup> acceptable for  $H_i$  and 23 Wm<sup>-2</sup> for  $H_d$ . Best case errors for instantaneous and daily fluxes in the literature are around 10–22 Wm<sup>-2</sup> (Kustas & Norman, 1996; Su, 2002) and can be up to 50%, even using sophisticated models, if the information required for parameterization is not available and several assumptions about surface characteristics have to be made.

Our results for  $NEF_d$  (non-evaporative fraction) are within the 0.10–0.20 RMSEs reported for the daily evaporative fraction  $EF_d$  ( $EF_d = 1 - NEF_d$ ) for the more complex parameterization of the SEBAL

**Table 5**  
Quantitative field validation of daily sensible heat flux ( $H_d$ ) in Wm<sup>-2</sup> estimated with ASTER data using *Retama*, *Anthyllis*, *Stipa*, shrubs, and lake surfaces

Date	Surface	Location	Field	ASTER	
			$H_d$ (Wm <sup>-2</sup> )	$H_d$ (Wm <sup>-2</sup> )	AE (Wm <sup>-2</sup> )
09-07-04	Shrubs	Llano Juanes	158.77	110.29	48.48
18-07-04	Shrubs	Llano Juanes	154.94	106.70	48.24
19-06-05	Shrubs	Llano Juanes	157.43	115.99	41.44
18-07-04	<i>Retama</i>	Rambla Honda	157.34	152.39	4.95
18-07-04	<i>Anthyllis</i>	Rambla Honda	133.15	139.38	6.24
18-07-04	<i>Stipa</i>	Rambla Honda	122.54	126.16	3.62
09-07-04	Lake	Greenhouses	0.00	-27.33	27.33
18-07-04	Lake	Greenhouses	0.00	-19.07	19.07
19-06-05	Lake	Greenhouses	0.00	7.06	7.06
	Std		74.70	71.12	
	MAE	22.94			
	RMSE	29.12			
	R	0.95			
	p	0.00009			

The column "Field" indicates  $H_d$  field estimates, and "ASTER" the  $H_d$  estimated using ASTER and ancillary data. AE is the absolute error (absolute difference between model and field observations). Std is the standard deviation of Field and ASTER estimates. The % Error is calculated as  $(H_{d,field} - H_{d,ASTER})100/H_{d,field}$ . For overall error evaluation, the MAE (mean absolute error), which is the average AE, the R (Pearson correlation coefficient), p (probability), of the regression between field and ASTER were calculated.

**Table 6**  
Quantitative field validation of the  $NEF_d$  (daily non-evaporative fraction), estimated with ASTER data using *Retama*, *Anthyllis*, *Stipa*, shrubs, and lake surfaces

Date	Surface	Location	Field	ASTER	
			$NEF_d$	$NEF_d$	AE
09-07-04	Shrubs	Llano Juanes	0.88	0.61	0.27
18-07-04	Shrubs	Llano Juanes	0.92	0.59	0.33
19-06-05	Shrubs	Llano Juanes	0.88	0.62	0.26
18-07-04	<i>Retama</i>	Rambla Honda	0.97	1.00	0.03
18-07-04	<i>Anthyllis</i>	Rambla Honda	0.83	0.89	0.06
18-07-04	<i>Stipa</i>	Rambla Honda	0.79	0.81	0.02
09-07-04	Lake ( $G_d=50$ )	Greenhouses	0.00	-0.17	0.17
09-07-04	Lake ( $G_d=-50$ )	Greenhouses		-0.11	0.11
18-07-04	Lake ( $G_d=50$ )	Greenhouses	0.00	-0.12	0.12
18-07-04	Lake ( $G_d=-50$ )	Greenhouses		-0.07	0.07
19-06-05	Lake ( $G_d=50$ )	Greenhouses	0.00	0.04	0.04
19-06-05	Lake ( $G_d=-50$ )	Greenhouses		0.02	0.02
	Std		0.44	0.45 (0.44)	
	MAE $G_d$ lake = 50 (-50)	0.14 (0.13)			
	RMSE $G_d$ lake = 50 (-50)	0.18 (0.17)			
	$R_{G_d}$ lake = 50 (-50)	0.94 (0.94)			
	$p_{G_d}$ lake = 50 (-50)	0.0002 (0.0002)			

The column "Field" indicates  $NEF_d$  field estimates, and "ASTER"  $NEF_d$  estimated using ASTER and ancillary data. AE is the absolute error (absolute difference between model and field observations). Two values for lake  $G_d$  (daily soil heat flux) were used for validation,  $G_{d, lake} = 50$  Wm<sup>-2</sup> and  $G_{d, lake} = -50$  Wm<sup>-2</sup>. Std is the standard deviation of Field and ASTER estimates. For overall error evaluation, the MAE (mean absolute error), which is the average AE, the R (Pearson correlation coefficient), p (probability) between field and ASTER data (n=9 observations) were calculated. The overall error was calculated twice, once with the dataset including the lake when  $G_{d, lake} = 50$  Wm<sup>-2</sup> and the other with the dataset including the lake when  $G_{d, lake} = -50$  Wm<sup>-2</sup> (in parentheses in the table).

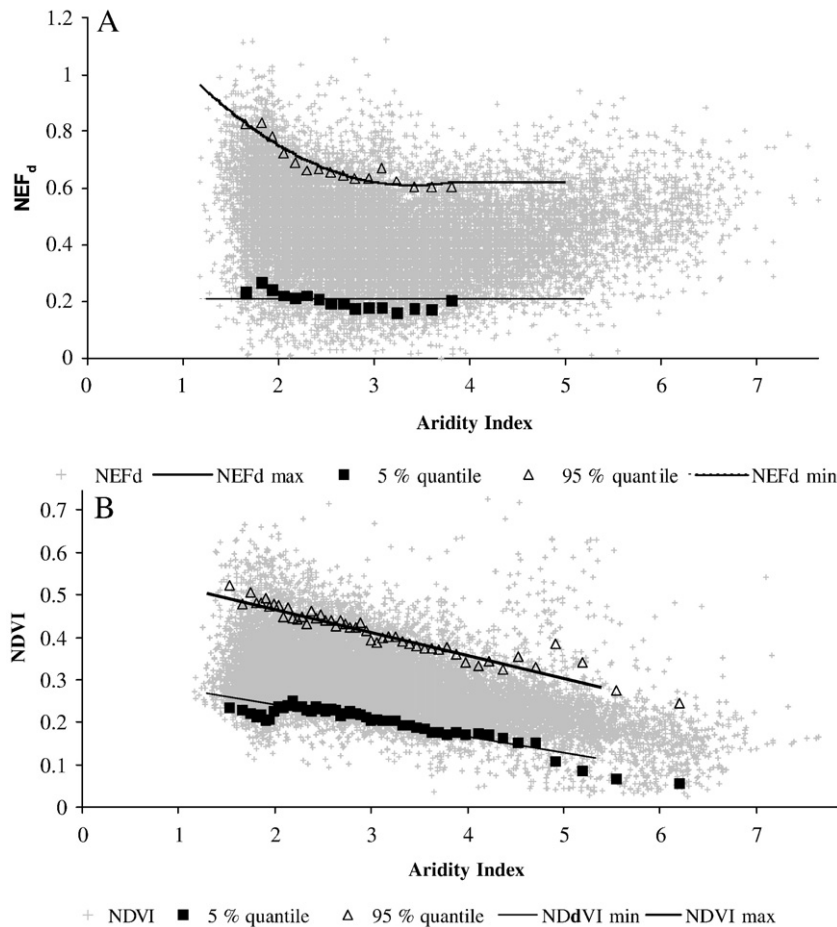


Fig. 5. Scatterplot for (A) NEF<sub>d</sub> vs AI (Aridity index) and (B) NDVI vs AI for July 18, 2004 in Sierra de Gádor. Quantile regression is shown for ecosystem boundary conditions using upper (95%) (solid squares) and lower (5%) quantiles (triangles).

model (Bastiaanssen et al., 1998b). Jiang and Islam (2001) found an RMSE for daily EF of 0.13, and Verstraeten et al., (2005) between 0.09–0.05 using S-SEBI in European forests compared to Euroflux data. Field validation shows that despite of the simplicity of the model, our results are within error ranges reported by other authors.

#### 4.2. Boundary conditions for ecosystem status and climatic type

The two land degradation indicators, NEFS and NDVIs, were calculated based on the two extremes (extremely disturbed and undisturbed) for ecosystem status and climate type. Fig. 5 shows the results for the July 18–2004 scene as an example.

Spatial patterns do not change much on different dates for the same indicator (Fig. 6). However, the spatial patterns from NDVIs and NEFs are correlated only to some extent. Higher NEFs and lower NDVIs should correspond to disturbed sites.

#### 4.3. Evaluation of land degradation risk indicators at severely disturbed sites

Evaluation of NEFs and NDVIs at sites that have undergone fire or human disturbances (see Fig. 1 for location), showed that NEFs at disturbed and control sites were close to 1 and 0, respectively, and vice-versa for NDVIs (Fig. 7). These results indicate that the methodology is successful, as, without supervision, it statistically identifies the extremes for ecosystem status for both indicators.

The hypothesis that disturbed sites should have a higher NEF<sub>d</sub> than undisturbed sites was confirmed with very significant differences ( $p < 0.001$ ) in NEF<sub>d</sub> from undisturbed sites ((Fig. 7). At this time of the year the only source of evapotranspiration would be canopy

transpiration, and therefore, the almost complete absence of vegetation cover produced a strong increase in the NEF<sub>d</sub>.

Disturbed and undisturbed sites may be located in different climatic regions, and therefore, it is preferable to perform direct spatial comparisons with the NEFS or NDVIs rather than with NDVI or NEF before rescaling. Comparisons showed significant mean differences in NDVIs and NEFS between disturbed and control sites, especially in the July 18–2004 image.

The key factor controlling NEFS responses in this case was vegetation greenness, as most of the variability in NEFS in this dataset is explained by NDVIS ( $R^2 = 0.7$  between NDVIs and NEFS;  $n = 780$ ;  $p < 0.001$ ) with 50–60% difference in NDVI between disturbed and undisturbed sites.

Results shown in Table 7 help understand the physical mechanisms producing changes in NEF<sub>d</sub> at disturbed sites. Lower vegetation greenness causes two main effects. First, there is a marked increase in  $T_{si}$  (Friedl & Davis, 1994; Bastiaanssen et al., 1998a), which enhances  $H_d$  transfer, as  $T_{ai}$  does not increase in the same proportion. Second, albedo increases due to a larger area of bare soil, which is dry at this time of the year. These two effects were the main controls for decreases in  $R_{nd}$  and compensated for the slightly higher levels observed in  $R_{si}$  (incoming shortwave radiation) at disturbed sites in summer.

Considering the surface energy balance equation  $\lambda E = R_{nd} - H$  (with  $G \approx 0$ ) (Kustas & Norman, 1996), and given the magnitude of the increases in  $H_d$  and decreases in  $R_{nd}$ , daily evapotranspiration ( $\lambda E_d$ ) should be significantly reduced at disturbed sites.

These findings are similar to responses attributed to land degradation in the Sahel (Dolman et al., 1997) and results from Arribas et al.

**Non-evaporative fraction standardized (NEFS)**

**NDVI standardized (NDVIS)**

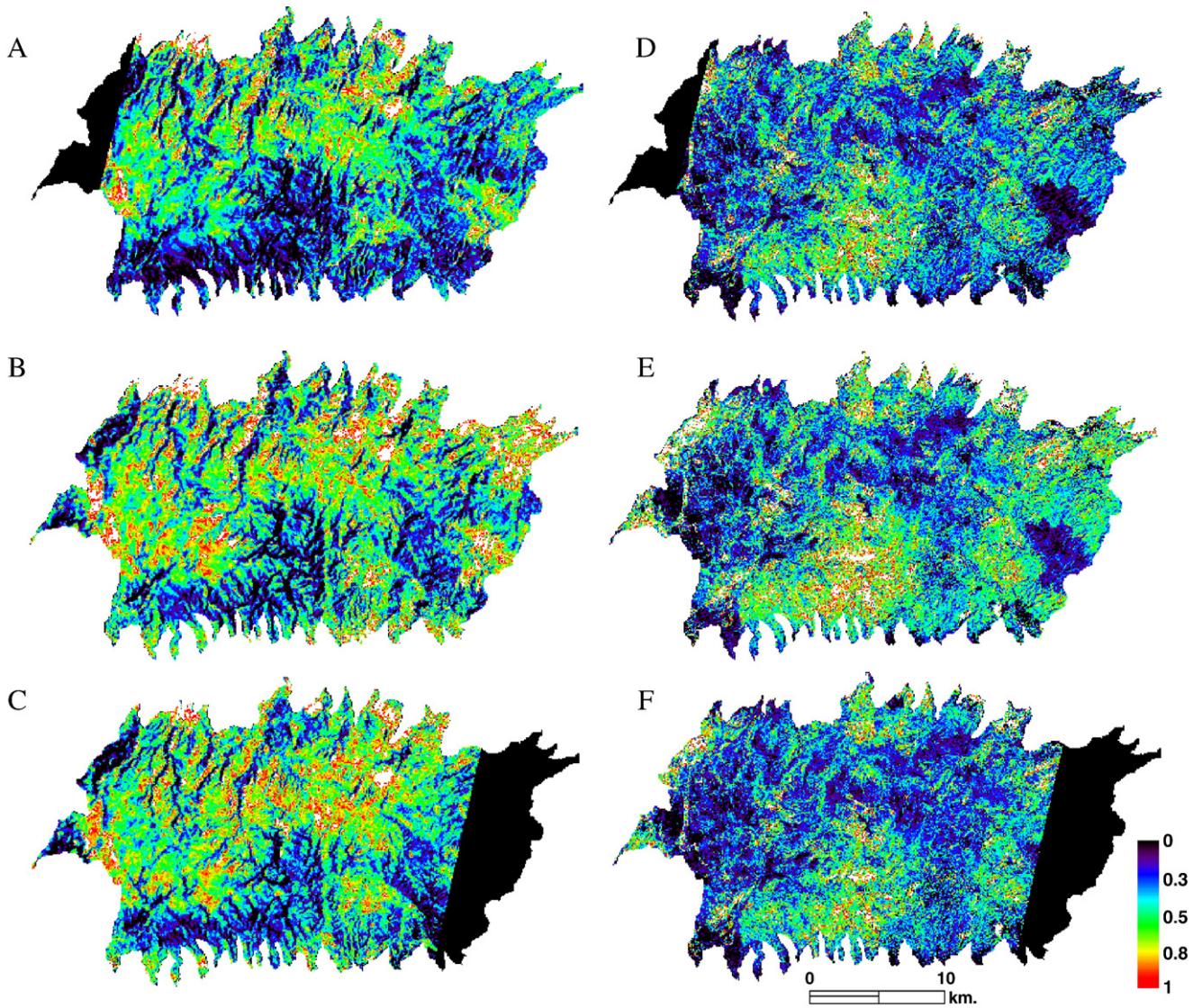


Fig. 6. NEFS (left panel) for 09-July-2004 (A), 18-July-2004 and (B), 19-June-2005 (C), and NDVIs (right panel) 09-July-2004 (D) 18-July-2004 and (E) 19-June-2005 (F) in Sierra de Gádor.

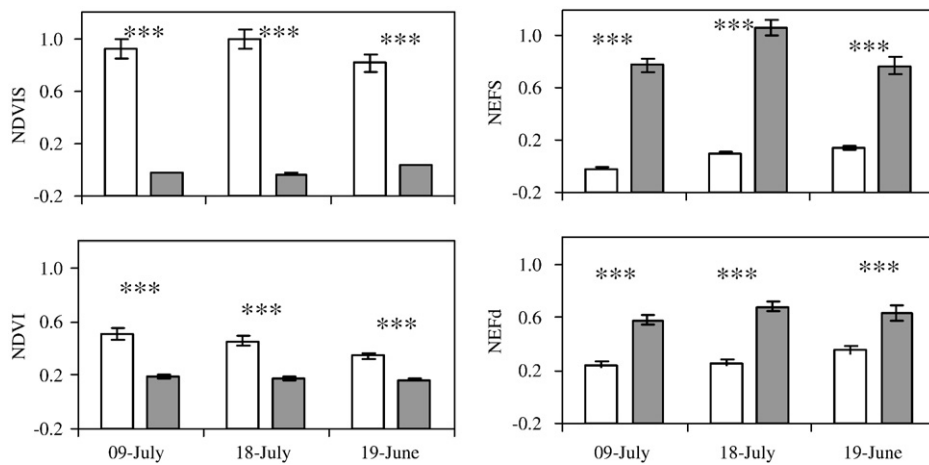


Fig. 7. Comparison of means at severely disturbed sites (gray bars), and control sites (white bars) on three dates. Significant mean differences have been tested (*t*-test for independent samples) between disturbed and control sites for NDVIs (NDVI standardized), NEFS (non-evaporative fraction standardized) NDVI and NEF<sub>d</sub> (daily non-evaporative fraction) within dates. Error bars represent within-site S.E (*n* = 80). Differences significant at *p* < 0.05, 0.01, 0.0001 are marked \*, \*\*, \*\*\*, respectively and non-significant differences by ns.

**Table 7**

Mean values for albedo, surface temperature ( $T_s$ ), air temperature ( $T_a$ ),  $T_s - T_a$ , daily sensible heat ( $H_d$ ), daily net radiation ( $R_{nd}$ ) and instantaneous incoming shortwave radiation ( $Rs_{\downarrow}$ ) at undisturbed sites and sites disturbed by severe fire or human activities

	Undisturbed	Disturbed	% change
	Mean $\pm$ SE	Mean $\pm$ SE	
<b>9-7-2004</b>			
Albedo	0.14 $\pm$ 0.01***	0.26 $\pm$ 0.02	77.46
$T_s$ ( $^{\circ}$ C)	30.09 $\pm$ 2.28***	39.73 $\pm$ 2.4	32.02
$T_a$ ( $^{\circ}$ C)	23.73 $\pm$ 1.8***	26.35 $\pm$ 1.59	11.04
$T_s - T_a$ ( $^{\circ}$ C)	6.37 $\pm$ 0.48***	13.38 $\pm$ 0.81	110.26
$H_d$ ( $Wm^{-2}$ )	42.08 $\pm$ 3.19***	88.49 $\pm$ 5.35	110.26
$R_{nd}$ ( $Wm^{-2}$ )	172.63 $\pm$ 13.09***	154.17 $\pm$ 9.31	-10.69
$Rs_{\downarrow}$ ( $Wm^{-2}$ )	852.83 $\pm$ 64.65***	933.9 $\pm$ 56.42	9.51
<b>18-07-2004</b>			
Albedo	0.17 $\pm$ 0.01***	0.26 $\pm$ 0.01	55.2
$T_s$ ( $^{\circ}$ C)	31.96 $\pm$ 2.44***	41.21 $\pm$ 2.19	28.94
$T_a$ ( $^{\circ}$ C)	25.69 $\pm$ 1.96***	26.37 $\pm$ 1.4	2.66
$T_s - T_a$ ( $^{\circ}$ C)	6.28 $\pm$ 0.48***	14.84 $\pm$ 0.79	136.5
$H_d$ ( $Wm^{-2}$ )	45.39 $\pm$ 3.47***	103.76 $\pm$ 5.51	128.57
$R_{nd}$ ( $Wm^{-2}$ )	168.82 $\pm$ 12.91***	153.21 $\pm$ 8.14	-9.24
$Rs_{\downarrow}$ ( $Wm^{-2}$ )	722.74 $\pm$ 55.27***	809.08 $\pm$ 43	11.95
<b>19-06-2005</b>			
Albedo	0.18 $\pm$ 0.01***	0.23 $\pm$ 0.02	28.2
$T_s$ ( $^{\circ}$ C)	36.07 $\pm$ 2.88***	42.85 $\pm$ 3.61	18.8
$T_a$ ( $^{\circ}$ C)	26.25 $\pm$ 2.09***	26.55 $\pm$ 2.24	1.14
$T_s - T_a$ ( $^{\circ}$ C)	9.82 $\pm$ 0.78 <sup>ns</sup>	16.3 $\pm$ 1.37	65.99
$H_d$ ( $Wm^{-2}$ )	69.57 $\pm$ 5.55***	115.48 $\pm$ 9.73	65.99
$R_{nd}$ ( $Wm^{-2}$ )	196.55 $\pm$ 15.69 <sup>ns</sup>	182.72 $\pm$ 15.39	-7.03
$Rs_{\downarrow}$ ( $Wm^{-2}$ )	859.64 $\pm$ 68.61***	838.21 $\pm$ 70.59	-2.49

Mean differences significant at  $p < 0.05, 0.01, 0.0001$  are marked by \*, \*\*, \*\*\* respectively, based on  $t$ -test for independent samples comparing means between disturbed and control sites. Non-significant differences are shown by ns. % change represents the percentage of change between disturbed and undisturbed sites.

(2003) on the sensitivity of climate and surface variables in a land degradation scenario in southeast Spain. Arribas et al. (2003) used a regional climate model coupled with a land surface model to evaluate the impact of land degradation simulated by changes in vegetation

cover, soil water holding capacity and albedo. Their model predicts changes in surface variables in the same direction and order of magnitude as ours, which is remarkable given the different approaches and coarser spatial resolution (25 km). They found decreases in the available energy for evapotranspiration ( $R_{nd} - G_d$ ), increases in  $T_{si}$  and  $T_{ai}$  proportional to the loss of vegetation cover, and increases in the Bowen ratio ( $\beta$ ). For instance, as the Bowen ratio ( $\beta = H/\lambda E$ ) is equivalent to  $\beta = NEF_d / (1 - NEF_d)$ , differences in  $\beta_{disturbed} - \beta_{undisturbed}$  at our study site were of 1.8, 1.0 and 1.2 (July 18, July 9 and June 19, respectively), while Arribas et al. (2003) found a mean difference of 2.0 for all southeast Spain in summer. Decreases in available energy ( $R_{nd} - G_d$ ) of 15  $Wm^{-2}$  found by Arribas et al., (2003) were similar to our results of 15.6, 18.4, and 13.8  $Wm^{-2}$  for July 18, July 9 and June 19, respectively.

4.4. Evaluation of land degradation risk indicators at disturbed soil sites

The effects of soil disturbance on surface energy partition and vegetation greenness were more subtle than those of fire or human disturbances. NDVI decreased from undisturbed to disturbed soil sites the same way regardless of lithological stratification. These decreases were greater in the NDVIS (significant at  $p < 0.001$ ), especially on marls in late summer (Fig. 8).

The behavior of  $NEF_d$  and  $NEFS$  is more complex (Fig. 8). Limestone samples presented the expected pattern of a higher  $NEF_d$  at disturbed sites, enhanced when using  $NEFS$ , especially in July 18-2004. However, on marl lithology, there were no significant differences ( $p < 0.01$ ) in  $NEF_d$  between disturbed and undisturbed sites. Furthermore, the land degradation indicator,  $NEFS$ , decreased at disturbed sites in late spring ( $p < 0.001$ ) and late summer ( $p < 0.05$ ).

Within each lithology, the pattern of AWC (Available Water Content) observed in Fig. 9 was better explained by NEF than by NDVI, suggesting that NEF not only responds to vegetation, but to differences in AWC, and is also influenced by other soil properties, as shown by its variation with lithology. Thus, while AWC at disturbed limestone sites is significantly lower than at control sites (and NEF is higher), differences in AWC and NEF between control and disturbed marl sites are not significant, despite the significant decrease observed in NDVI.

However, AWC alone cannot fully explain NEF interactions with lithology. Thus, AWC levels suggest that NEF at marl sites should be

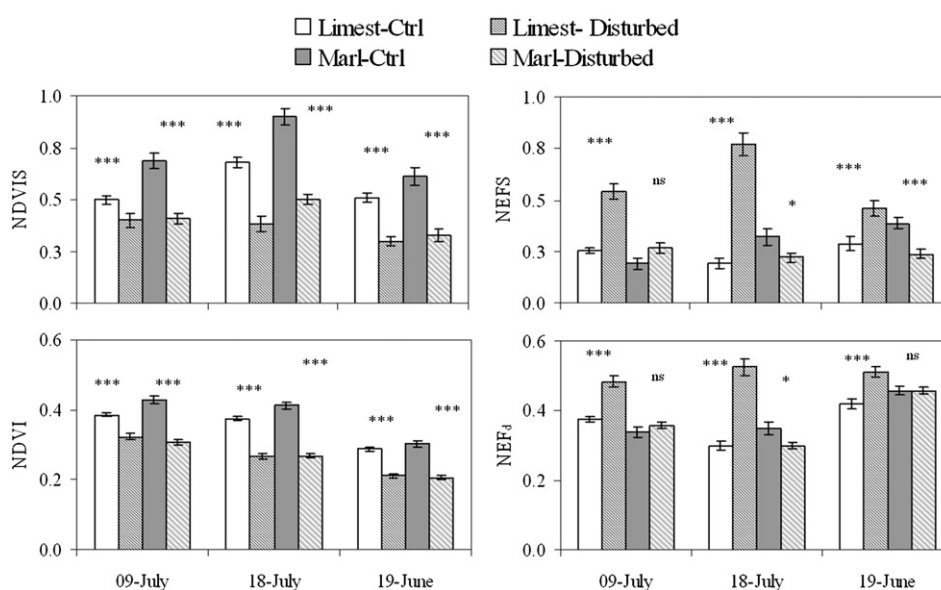


**Fig. 8.** Comparison of means at disturbed soil sites and undisturbed (Ctrl) soil sites stratified by geology, limestone (limest) or marls (Marl), on three dates. Significant mean differences have been tested ( $t$ -test for independent samples) for NDVIS (NDVI standardized), NEFS (non-evaporative fraction standardized) NDVI and  $NEF_d$  (daily non-evaporative fraction) within dates. Error bars represent within-site S.E. ( $n=80$ ). Differences significant at  $p < 0.05, 0.01, 0.0001$  are marked \*, \*\*, \*\*\*, respectively and non-significant differences by ns.

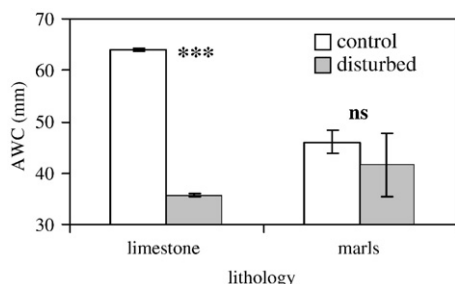


**Fig. 9.** Available Water Content (AWC) in mm of disturbed soil sites affected by losses of topsoil organic matter (mollic horizon) and at control sites on limestone and marl lithology. Error bars represent the confidence interval at  $p < 0.05$  for the  $t$ -distribution (1.96·SE). Differences significant ( $t$ -test for independent samples) at  $p < 0.0001$  are marked by \*\*\*, and non-significant differences by ns.

higher. For instance, despite similar AWC at disturbed marl and limestone sites, NEF and NEFS at marl sites are significantly higher (Fig. 9). This could be because calcschist/marl is more plastic than limestone bedrock, allowing deeper root growth and a higher soil water-holding capacity in the saprolite zone than limestone with lythic contact between soil and rock (Stolt & Baker, 1994).

Furthermore, AWC was estimated following standard procedures based only on soil volume of the fine-earth fraction to avoid overestimating available water. In such analyses, the gravel fraction is usually assumed to have no water retention capacity, and its contribution to total water storage capacity is ignored. In the Sierra de Gador the contribution to water retention by gravel can represent a considerable proportion (10–20%) of the AWC for plant growth, especially in the case of marl soils (Oyonarte et al., 1998).

A higher soil water reserve in marls could also explain the lower  $T_{si}$  observed on marls, despite the fact that disturbed soil sites on both

types of lithology, especially marls, are subject to higher levels of incoming shortwave radiation ( $Rs_{i\downarrow}$ ) (Table 8). Consequently,  $Rn_d$  increases at disturbed marl sites, while it does not change or even decreases on limestone. In marls, increases in albedo and  $T_{si}$  are not enough to compensate for higher insolation, resulting in a non-significant change in  $H_d$  ( $p < 0.01$ ).

According to our results, marl and limestone disturbed sites present different energy partitioning into  $\lambda E$  and  $H_d$ . Because  $\lambda E_d \approx Rn_d - H_d$ , on limestone-soil disturbed sites, the increase in  $H_d$  and the absence of change or decrease in  $Rn_d$  results in a reduction in  $\lambda E_d$  similar to severely disturbed sites. In contrast, on marl disturbed soil sites there is a slight increase in  $Rn_d$  that has to be dissipated, mainly through a slight increase in  $\lambda E_d$ , as  $H_d$  does not change significantly ( $p < 0.01$ ) (Table 8). It seems plausible that transpiration from the remaining vegetated fraction on marls can be enhanced due to increases in  $H_d$  as reported by Kabat et al. (1997) in the Sahel; and depending on the magnitude of this increase and the surface properties (soil, vegetation type) aggregated  $\lambda E$  at the pixel level could be similar or even greater than at sites with intact horizons. It is known that advection of heat between warm soil and cool vegetation results in an increase in canopy transpiration, being stronger advection when surface heterogeneity increases and when the difference between vegetation and soil temperature is wider (Shuttleworth & Wallace, 1985). This issue will be studied further in the future using more refined models.

Our results also suggest that marl sites receiving higher insolation rates are more vulnerable to lose surface soil horizons because they are subjected to more extreme drought conditions in an already arid environment, as indicated by higher  $Rs_{i\downarrow}$  at those sites (Table 8). Austin & Vivanco (2006) showed that in water-limited ecosystems, the only factor with a significant effect on carbon turnover was solar radiation via photodegradation which could explain a greater vulnerability to soil degradation.

For this dataset, the two indicators provide different information, in contrast to severely disturbed sites, with decoupling of NDVIS and

**Table 8**  
Mean values for albedo, surface temperature ( $T_{si}$ ), air temperature ( $T_{ai}$ ),  $T_{si} - T_{ai}$ , daily sensible heat ( $H_d$ ), daily net radiation ( $Rn_d$ ) and instantaneous incoming shortwave radiation ( $Rs_{i\downarrow}$ ) at disturbed and undisturbed soil sites affected by surface horizon loss stratified by the two dominant geological types: limestone and marl

	Limestone sites			Marl sites		
	Undisturbed	Disturbed	% change	Undisturbed	Disturbed	% change
	Mean±SE	Mean±SE		Mean±SE	Mean±SE	
<b>09-07-04</b>						
Albedo	0.16±0.001***	0.17±0.002	8.28	0.15±0.002***	0.17±0.003	14.19
$T_{si}$ (°C)	33.32±0.23***	37.95±0.36	13.89	34.13±0.31***	36.40±0.19	6.65
$T_{ai}$ (°C)	23.99±0.19***	25.99±0.14	8.35	25.55±0.14***	26.88±0.15	5.19
$T_{si} - T_{ai}$ (°C)	9.33±0.21***	11.96±0.39	28.13	8.58±0.33*	9.53±0.23	10.99
$H_d$ ( $Wm^{-2}$ )	61.72±1.39***	79.08±2.6	28.13	56.76±2.20*	62.99±1.51	10.99
$Rn_d$ ( $Wm^{-2}$ )	164.40±2.52 ns	165.1±1.55	0.42	167.99±1.99***	178.33±1.86	6.16
$Rs_{i\downarrow}$ ( $Wm^{-2}$ )	847.35±12.07*	881.55±7.41	4.04	846.00±9.59***	912.15±7.01	7.82
<b>18-07-04</b>						
Albedo	0.17±0.002***	0.19±0.002	10.47	0.16±0.002***	0.19±0.002	16.67
$T_{si}$ (°C)	33.41±0.27***	37.88±0.37	13.38	34.24±0.38 ns	34.87±0.18	1.85
$T_{ai}$ (°C)	25.97±0.1***	27.05±0.07	4.13	26.68±0.07***	27.48±0.07	3.02
$T_{si} - T_{ai}$ (°C)	7.44±0.29***	10.91±0.39	46.61	7.476±0.41 ns	7.47±0.19	-0.12
$H_d$ ( $Wm^{-2}$ )	50.56±2.07***	79.33±2.59	56.91	57.23±2.96 ns	53.6±1.44	-7.23
$Rn_d$ ( $Wm^{-2}$ )	168.73±2.05***	157.87±2.21	-6.44	163.36±1.73***	179.43±1.24	9.84
$Rs_{i\downarrow}$ ( $Wm^{-2}$ )	715.5±11.23 ns	739.8±6.37	3.40	707.4±8.38***	786.15±4.64	11.13
<b>19-06-05</b>						
Albedo	0.18±0.002***	0.205±0.002	11.41	0.19±0.002***	0.206±0.002	11.96
$T_{si}$ (°C)	37.68±0.28***	41.95±0.4	11.33	40.54±0.34 ns	41.14±0.24	1.47
$T_{ai}$ (°C)	27.12±0.15***	28.74±0.02	5.99	28.30±0.07***	28.80±0	1.77
$T_{si} - T_{ai}$ (°C)	10.56±0.28***	13.21±0.4	25.04	12.24±0.35 ns	12.33±0.24	0.77
$H_d$ ( $Wm^{-2}$ )	74.82±2.00***	93.55±2.85	25.04	86.7±2.50 ns	87.37±1.68	0.77
$Rn_d$ ( $Wm^{-2}$ )	183.70±3.09 ns	182.13±1.59	-0.85	188.75±1.32 ns	191.96±1.07	1.70
$Rs_{i\downarrow}$ ( $Wm^{-2}$ )	939.6±14.19 ns	964.8±9.76	2.68	974.25±8.28**	1002.15±5.26	2.86

Mean differences significant at  $p < 0.05$ , 0.01, 0.0001 are marked \*, \*\*, \*\*\*, respectively, based on  $t$ -test for independent samples comparing means between disturbed and control sites. Non-significant differences are marked ns. % change is the percentage of change between degraded and non-degraded sites.

NEFS as shown by low  $R^2$  between NDVIS and NEFS ( $R^2_{\text{limestone}}=0.30$ ;  $p<0.0001$  and  $R^2_{\text{marls}}=0.12$ ;  $p<0.0001$ ). Soil properties and not just vegetation greenness play a significant role in the surface energy balance.

#### 4.5. Monitoring land degradation risk using NEFS and NDVIS

Fig. 10 shows the scatter plot of NDVIS and NEFS on the three dates with field samples for evaluating land degradation overlaid. As was hypothesized in Fig. 2, pixels near the top of the y axis and left of the x axis are significantly different from control values for both indicators should present a high risk of land degradation (e.g., land use-land cover changes are located at this end) as both indicators detect signs of degradation (Fig. 10).

The two indicators, NEFS and NDVIS, provide different information on land condition. In general, the stronger the disturbance is, the greater the decrease in NDVIS and increase in NEFS. There is a gradient of states from undisturbed sites (low risk of degradation) to sites with significant differences with respect to undisturbed sites (high risk of degradation), at which either NDVIS or NEFS can have a dominant effect, with non-abrupt transitions in some cases (e.g., undisturbed limestone and disturbed marls). In general, NDVIS greater than 1 or NEFS much below 0 are associated with irrigated orchards. NDVIS below 0 and NEFS over 1 are associated with sites altered by humans without vegetation, such as urban areas, roads, or barren land. An NDVIS below 1 with relatively high NEFS is mainly associated with high-albedo greenhouses where ventilation releases high concentrations of water vapor.

Although there is a general trend toward increasing NEFS with decreasing NDVIS, there is also considerable scatter (Fig. 10). Their relationship depends on many factors affecting the  $NEF_d$  and NDVI not evaluated in this work, such as vegetation water-use strategy, aerodynamic roughness, and spatial distribution of vegetation within the pixel among others.

This study provides a methodology for detecting disturbed sites that could be at risk of land degradation. It does not pretend to identify the drivers of such disturbances or whether loss of functionality detected at hot-spots or sites at risk of degradation is irreversible (desertification), which would require long-term analyses (Paruolo et al., 2000). Nonetheless, the methodology proposed, if included as part of a long-term monitoring system might contribute to a proactive land degradation management. Land degradation assessments using retrospective remote sensing time series have not been very successful from a management perspective due to the high costs involved in ecosystem restoration programs once degradation has already taken place (Puigdefábregas, 1998).

## 5. Conclusions

This study presents a simple methodology to monitor land degradation risk by detecting disturbed sites for regional-scale application. It is based on the use of snapshots of two complementary indicators: the standardized non-evaporative fraction (NEFs), and the standardized NDVI (NDVIS). The non-evaporative fraction is related to ecosystem water use through the partition of the surface energy into latent and sensible heat flux, and NDVI to vegetation greenness.

Both indices were computed from ASTER data. The  $NEF_d$  was estimated using a simple surface energy balance model with validation results comparable to other studies ( $R^2=0.88$ ;  $RMSE=0.18$ ,  $p<0.0001$ ). To allow spatial comparisons across different climatic contexts  $NEF_d$  and NDVI were rescaled for each level of aridity between two possible extremes for ecosystem status: extremely disturbed and undisturbed. These extremes were found statistically using quantile regression (5% and 95%) with the aridity index. Results show that NEFS values at ground truth sites associated with the extremes (preserved and extremely disturbed) were close to 1 and 0, and vice-versa for NDVIS indicating that

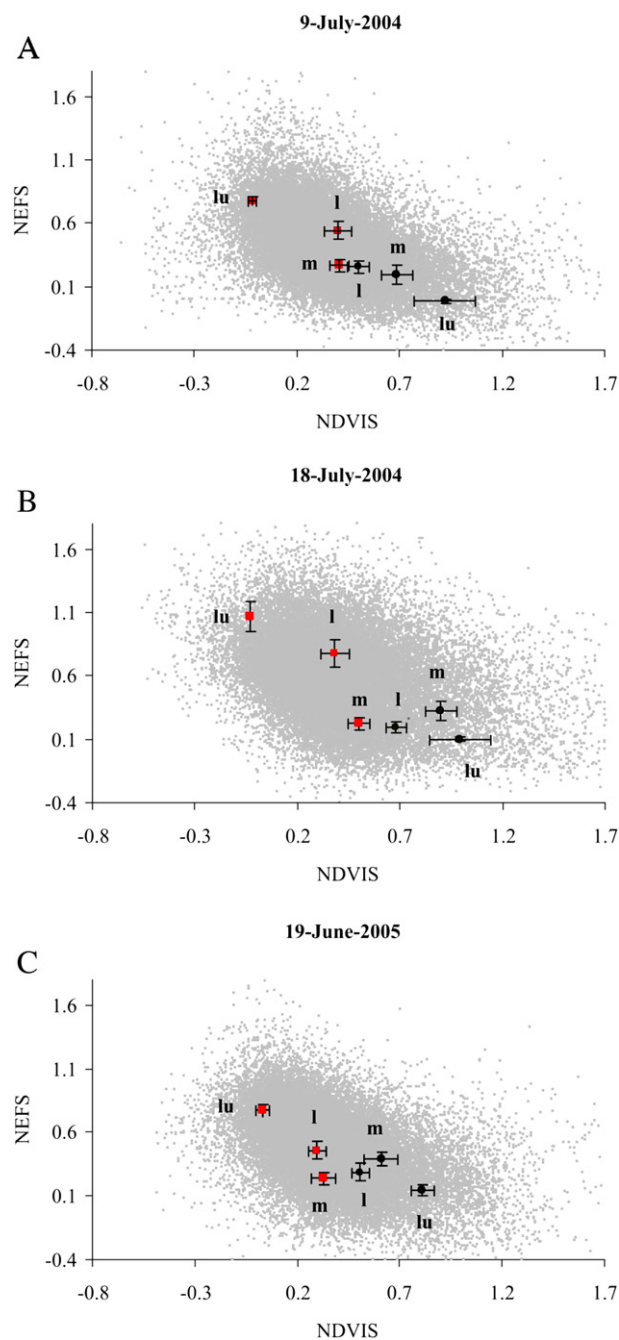


Fig. 10. Scatter plot of NDVIS (standardized NDVI) versus NEFS (Standardized non-evaporative fraction) for all the pixels in the study site (gray points) on A) 9 July 2004, B) 18 July 2004 and C) 19 June 2005. Overlaid red squares are the sample means at disturbed sites for land use changes (lu), soil disturbed on marls sites (m), and soil disturbed on limestone sites (l). Overlaid black dots are control sites means for land use (lu), marl sites (m), and limestone sites (l). Error bars represent within-site S.E.

the methodology is successful in identification of ecosystem status extremes (boundaries) without supervision.

The hypothesis that disturbed sites, at risk of land degradation, should have significantly higher NEFS than undisturbed ones was supported at severely disturbed ground truth sites affected by fire and land use changes. At sites affected by loss of topsoil organic matter, NEFS was significantly higher than in undisturbed soils located at limestone sites but not at disturbed marl/calcschist soils. Available water capacity (AWC) was found to be similar between disturbed and control marl sites, but was significantly lower than control at disturbed limestone sites. These results suggest that NEFS is influenced more by other soil properties such as the soil water reserve.

These results suggest that an NDVIS significantly lower than the control is clearly symptomatic of land degradation risk. However the NEFS can provide additional information on the surface water deficit, including the role of soil properties in regulating surface water and energy exchanges.

Results from this work also highlight some of the changes in surface properties affecting energy exchanges taking place at disturbed sites, with findings similar to other studies. In general, disturbed sites presented lower vegetation greenness, and higher albedo and surface temperature, leading to increased sensible heat flux and lower or no changes in net radiation. In this study, the magnitude of changes was dependent on disturbance type and date, being greater for the late summer scene and at sites affected by severe anthropogenic land use changes.

These results have implications, not only for identification of disturbed areas, at risk of land degradation, but also for evaluating the impact of disturbances on the hydrological cycle, and possible feedback effects on climate if disturbances occur over large spatial scales. This methodology, if applied for continuous monitoring can provide information about temporal trends and ecosystem resilience or land degradation. Future research should focus in refinement of the NEF<sub>d</sub> model, and establishing degradation thresholds with the indicators for land degradation risk mapping.

### Acknowledgements

This study received financial support from several different research projects: the integrated EU project, DeSurvey (A Surveillance System for Assessing and Monitoring of Desertification) (ref.: FP6-00.950, contract no. 003950), the PROBASE (ref.: CGL2006-11619/HID) and CANOA (ref.: CGL2004-04919-C02-01/HID) projects funded by the Spanish Ministry of Education and Science; and the BACAEMA ('Balance de carbono y de agua en ecosistemas de matorral mediterráneo en Andalucía: Efecto del cambio climático', RNM-332) and CAMBIO ('Efectos del cambio global sobre la biodiversidad y el funcionamiento ecosistémico mediante la identificación de áreas sensibles y de referencia en el SE ibérico', RNM 1280) projects funded by the Junta de Andalucía (Andalusian Regional Government). The authors wish to thank Dr. Were, Dr. Litago and Angeles Ruiz for helpful discussions, S.Vidal and R.Ordiales for IT assistance, Alfredo Durán for field assistance, and Deborah Fuldauer for improving the English text. The helpful comments and advise from two anonymous reviewers are gratefully acknowledged.

### References

- Abrams, M., & Hook, S. (2002). ASTER user handbook version 2. *NASA JPL* (pp. 100–109). 2002.
- Aldaya, F., Baena, J., & Ewert, K. (1977). Mapa Geológico de España. *Serie MAGNA (E 1:50.000). Hoja 1.043-Berja*. IGME Madrid, Spain: Servicio Publicaciones Ministerio Industria y Energía.
- Arribas, A., Gallardo, C., Gaertner, M. A., & Castro, M. (2003). Sensitivity of the Iberian Peninsula climate to a land degradation. *Climate Dynamics*, 20, 477–489.
- Asner, G. P., Borghi, C. E., & Ojeda, R. A. (2003). Desertification in Central Argentina: changes in ecosystem carbon and nitrogen from imaging spectroscopy. *Ecological Applications*, 13, 629–648.
- Austin, A. T., & Vivanco, L. (2006). Plant litter decomposition in a semi-arid ecosystem controlled by photodegradation. *Nature*, 442, 555–558.
- Baldocchi, D., Falge, E., Gu, L. H., Olson, R., Hollinger, D., Running, S., et al. (2001). FLUXNET: a new tool to study the temporal and spatial variability of ecosystem-scale carbon dioxide, water vapor, and energy flux densities. *Bulletin of the American Meteorological Society*, 82, 2415–2434.
- Bastiaanssen, W. G. M., Menenti, M., Feddes, R. A., & Holtslag, A. A. M. (1998). A remote sensing surface energy balance algorithm for land (SEBAL) — 1. Formulation. *Journal of Hydrology*, 213, 198–212.
- Bastiaanssen, W. G. M., Pelgrum, H., Wang, J., Ma, Y., Moreno, J. F., Roerink, G. J., et al. (1998). A remote sensing surface energy balance algorithm for land (SEBAL) — 2. Validation. *Journal of Hydrology*, 213, 213–229.
- Bisht, G., Venturini, V., Islam, S., & Jiang, L. (2005). Estimation of the net radiation using MODIS (Moderate Resolution Imaging Spectroradiometer) data for clear sky days. *Remote Sensing of Environment*, 97, 52–67.
- Boer, M. M., & Puigdefábregas, J. (2003). Predicting potential vegetation index values as a reference for the assessment and monitoring of dryland condition. *International Journal of Remote Sensing*, 24, 1135–1141.
- Boer, M. M., & Puigdefábregas, J. (2005). Assessment of dryland condition using spatial anomalies of vegetation index values. *International Journal of Remote Sensing*, 26, 4045–4065.
- Bolle, H. J., Andre, J. C., Arrue, J. L., Barth, H. K., Bessemoulin, P., Brasa, A., et al. (1993). EFEDA — European Field Experiment in A Desertification-Threatened Area. *Annales Geophysicae-Atmospheres Hydrospheres and Space Sciences*, 11, 173–189.
- Burba, G. G., Verma, S. B., & Kim, J. (1999). Energy fluxes of an open water area in a mid-latitude prairie wetland. *Boundary-Layer Meteorology*, 91, 495–504.
- Carlson, T. N., Capehart, W. J., & Gillies, R. R. (1995). A new look at the simplified method for remote sensing of daily evapotranspiration. *Remote Sensing of Environment*, 54, 161–167.
- Caselles, V., Artigao, M. M., Hurtado, E., Coll, C., & Brasa, A. (1998). Mapping actual evapotranspiration by combining Landsat TM and NOAA-AVHRR images: application to the Barrax area, Albacete, Spain. *Remote Sensing of Environment*, 63, 1–10.
- Chehbouni, A., Goodrich, D. C., Moran, M. S., Watts, C. J., Kerr, Y. H., Dedieu, G., et al. (2000). A preliminary synthesis of major scientific results during the SALSA program. *Agricultural and Forest Meteorology*, 105, 311–323.
- Contreras, S. (2006). Spatial distribution of the annual water balance in semiarid mountainous regions. Application to Sierra de Gádor (Almería, SE Spain) (in Spanish). PhD dissertation, CD-Rom. Servicio de Publicaciones de la Universidad de Almería (Spain).
- Czajkowski, K. P., Goward, S. N., Mulhern, T., Goetz, S. J., Walz, A., Shirey, D., et al. (2000). Estimating environmental variables using thermal remote sensing. In D. A. Quattrochi, & J. C. Luvall (Eds.), *Thermal remote sensing in land surface processes* (pp. 11–32). Boca Raton, Florida: CRC Press.
- Dall'Omo, G., & Karnieli, A. (2002). Monitoring phenological cycles of desert ecosystems using NDVI and LST data derived from NOAA-AVHRR imagery. *International Journal of Remote Sensing*, 23, 4055–4071.
- Dazzi, C., & Monteleone, S. (1998). Consequences of human activities on pedodiversity of soils: a case study in a vineyard area in south-east Sicily (Italy). *Proceedings of the 16th World Congress of Soil Sciences Montpellier, France: ISSS CD-ROM*.
- Dolman, A. J., Gash, J. H. C., Goutorbe, J. P., Kerr, Y., Lebel, T., Prince, S. D., et al. (1997). The role of the land surface in Sahelian climate: HAPEX-Sahel results and future research needs. *Journal of Hydrology*, 189, 1067–1079.
- Domingo, F., Villagarcía, L., Brenner, A. J., & Puigdefábregas, J. (1999). Evapotranspiration model for semi-arid shrub-lands tested against data from SE Spain. *Agricultural and Forest Meteorology*, 95, 67–84.
- French, A. N., Jacob, F., Anderson, M. C., Kustas, W. P., Timmermans, W., Gieske, A., et al. (2005). Surface energy fluxes with the Advanced Spaceborne Thermal Emission and Reflection radiometer (ASTER) at the Iowa 2002 SMACEX site (USA). *Remote Sensing of Environment*, 99, 55–65.
- Friedl, M. A., & Davis, F. W. (1994). Sources of variation in radiometric surface-temperature over a tallgrass prairie. *Remote Sensing of Environment*, 48, 1–17.
- Fu, P. D., & Rich, P. M. (2002). A geometric solar radiation model with applications in agriculture and forestry. *Computers and Electronics in Agriculture*, 37, 25–35.
- Gamon, J. A., Field, C. B., Goulden, M. L., Griffin, K. L., Hartley, A. E., Joel, G., et al. (1995). Relationships between NDVI, canopy structure, and photosynthesis in 3 Californian vegetation types. *Ecological Applications*, 5, 28–41.
- García, M., Villagarcía, L., Contreras, S., Domingo, F., & Puigdefábregas, J. (2007). Comparison of three operative models for estimating the surface water deficit using ASTER reflective and thermal data. *Sensors*, 7, 860–883.
- Gillespie, A., Rokugawa, S., Matsunaga, T., Cothren, J. S., Hook, S., & Kahle, A. B. (1998). A temperature and emissivity separation algorithm for advanced spaceborne thermal emission and reflection radiometer (ASTER) images. (1998). *IEEE Transactions of Geoscience and Remote Sensing*, 36, 1113–1126.
- Gómez, M., Olioso, A., Sobrino, J. A., & Jacob, F. (2005). Retrieval of evapotranspiration over the Alpillles/ReSeDA experimental site using airborne POLDER sensor and a thermal camera. *Remote Sensing of Environment*, 96, 399–408.
- Goutorbe, J. P., Lebel, T., Dolman, A. J., Gash, J. H. C., Kabat, P., Kerr, Y. H., et al. (1997). An overview of HAPEX-Sahel: a study in climate and desertification. *Journal of Hydrology*, 189, 4–17.
- Grossman, R. B. (1983). Entisols. Pedogenesis and soil taxonomy. Part II. The Soil orders. In L. P. Wilding, N. E. Smeck, & G. F. Hall (Eds.), *Developments in Soil Science* (pp. 55–90). Amsternsdam: Elsevier.
- Gurney, R. J., & Sewell, I. J. (1997). Observation and simulation of energy budgets at the surface of a prairie grassland. In P. R. Van Gardingen, G. M. Foody, & P. J. Curran (Eds.), *Scaling-up: from cell to landscape* (pp. 319–346). Cambridge, UK: Cambridge University Press.
- Hall, F. G., Huemmrich, K. F., Goetz, S. J., Sellers, P. J., & Nickeson, J. E. (1992). Satellite remote sensing of surface energy balance — success, failures, and unresolved issues in FIFE. *Journal of Geophysical Research-Atmospheres*, 97, 19061–19089.
- Hargreaves, G. H., & Samani, Z. A. (1982). Estimating potential evapotranspiration. *ASCE Journal of Irrigation and Drainage Engineering*, 108, 225–230.
- Hasse, P., Pignaire, F. I., Clark, S. C., & Incoll, L. D. (2000). Photosynthetic rate and canopy development in the drought-deciduous shrub *Anthyllis cytisoides* L. *Journal of Arid Environments*, 46, 79–91.
- Holm, A. M., Cridland, S. W., & Roderick, M. L. (2003). The use of time-integrated NOAA NDVI data and rainfall to assess landscape degradation in the arid shrubland of Western Australia. *Remote Sensing of Environment*, 85, 145–158.
- Hurtado, E., & Sobrino, J. A. (2001). Daily net radiation estimated from air temperature and NOAA AVHRR data: a case study for the Iberian Peninsula. *International Journal of Remote Sensing*, 22(8), 1521–1533.
- Ibáñez, J. J., Bello, A., & García-Álvarez, A. (2005). La conservación de los suelos Europeos. Un análisis crítico de la actual estrategia de la Unión Europea. *Protección del Suelo y el Desarrollo Sostenible Serie Medio Ambiente, Vol 6*. (pp. 133–161) Madrid: Publicaciones del IGME, MEC.

- Idso, S. B., & Jackson, R. D. (1969). Thermal radiation from the Atmosphere. *Journal of Geophysical Research*, 74, 5397–5403.
- Jackson, R. D., Moran, M. S., Gay, L. W., & Raymond, L. H. (1987). Evaluating evaporation from field crops using airborne radiometry and ground-based meteorological data. *Irrigation Science*, 8, 81–90.
- Jackson, R. D., Reginato, R. J., & Idso, S. B. (1977). Wheat canopy temperature – practical tool for evaluating water requirements. *Water Resources Research*, 13, 651–656.
- Jacob, F., Olioso, A., Gu, X. F., Su, Z. B., & Seguin, B. (2002). Mapping surface fluxes using airborne visible, near infrared, thermal infrared remote sensing data and a spatialized surface energy balance model. *Agronomie*, 22, 669–680.
- Jiang, L., & Islam, S. (2001). Estimation of surface evaporation map over southern Great Plains using remote sensing data. *Water Resources Research*, 37, 329–340.
- Kabat, P., Dolman, A. J., & Elbers, J. A. (1997). Evaporation, sensible heat and canopy conductance of fallow savannah and patterned woodland in the Sahel. *Journal of Hydrology*, 189, 494–515.
- Koenker, R., & Hallock, K. F. (2001). Quantile regression. *Journal of Economic Perspectives*, 15, 143–156.
- Kustas, W. P., & Norman, J. M. (1996). Use of remote sensing for evapotranspiration monitoring over land surfaces. *Hydrological Sciences Journal-Journal des Sciences Hydrologiques*, 41, 495–516.
- Kustas, W. P., Perry, E. M., Doraiswamy, P. C., & Moran, M. S. (1994). Using satellite remote sensing to extrapolate evapotranspiration estimates in time and space over a semiarid rangeland basin. *Remote Sensing of Environment*, 49, 275–286.
- Lambin, E. F. (1996). Change detection at multiple temporal scales: seasonal and annual variations in landscape variables. *Photogrammetric Engineering and Remote Sensing*, 62, 931–938.
- Lambin, E. F., & Ehrlich, D. (1997). Land-cover changes in sub-Saharan Africa (1982–1991): application of a change index based on remotely sensed surface temperature and vegetation indices at a continental scale. *Remote Sensing of Environment*, 61, 181–200.
- LeHouerou, H. N. (1996). Climate change, drought and desertification. *Journal of Arid Environments*, 34, 133–185.
- Li, X.-Y., Contreras, S., & Solé-Benet, A. (2007). A spatial distribution of rock fragments in dolines: a case study in a semiarid Mediterranean mountain-range (Sierra Gádor, SE Spain). *Catena*, 70(3), 336–374.
- Liang, S. L. (2001). Narrowband to broadband conversions of land surface albedo I Algorithms. *Remote Sensing of Environment*, 76, 213–238.
- Liu, H. P., Randerson, J. T., Lindfors, J., & Chapin, F. S. (2005). Changes in the surface energy budget after fire in boreal ecosystems of interior Alaska: an annual perspective. *Journal of Geophysical Research-Atmospheres*, 110, D13101.
- López-Bermúdez, F., Boix-Fayos, C., Solé-Benet, A., Albaladejo, J., Barberá, G. C., del Barrio, G., et al. (2005). Landscapes and desertification in South-East Spain: overview and field sites. *Field Trip Guide. A-5.6th International conference on Geomorphology* (pp. 18–23). Sociedad Española de Geomorfología.
- Ludwig, J. A., & Tongway, D. J. (2000). Viewing rangelands as landscape systems. In O. Arnalds, & S. Archer (Eds.), *Rangeland Desertification* (pp. 39–52). Dordrecht, the Netherlands: Kluwer Academic Publishers.
- Mildrexler, D. J., Zhao, M. S., Heinsch, F. A., & Running, S. W. (2007). A new satellite-based methodology for continental-scale disturbance detection. *Ecological Applications*, 17, 235–250.
- Nemani, R., & Running, S. W. (1997). Land cover characterization using multitemporal Red, Near-IR, and Thermal-IR data from NOAA/AVHRR. *Ecological Applications*, 7, 79–90.
- Nicholson, S. (2000). Land surface processes and Sahel climate. *Reviews of Geophysics*, 38, 117–139.
- Nie, D., Flitcroft, I. D., & Kanemasu, E. T. (1992). Performance of Bowen-ratio systems on a slope. *Agricultural and Forest Meteorology*, 59, 165–181.
- Okin, G. S. (2002). Toward a unified view of biophysical land degradation processes in arid and semi-arid lands. In J. F. Reynolds, & D. M. Stafford Smith (Eds.), *Global Desertification: Do Humans Cause Deserts?* (pp. 95–109). Berlin: Dahlem University Press.
- Oswald, C. J., & Rouse, W. R. (2004). Thermal characteristics and energy balance of various-size Canadian Shield lakes in the Mackenzie River basin. *Journal of Hydrometeorology*, 5, 129–144.
- Oyonarte, C., Muñoz, M., & Delgado, R. (2008). El paisaje edáfico. In Oyonarte, C., Gimenez, E., & Villalobos, M. (Eds.), *Sierra de Gádor. Patrimonio Natural y Cultural*. (pp. 69–90). Fundación Gypaetus Ed. Sevilla.
- Oyonarte, C. (1992). Estudio Edáfico de la Sierra de Gádor (Almería). Evaluación para usos forestales. PhD thesis. 712 pp. Universidad de Granada.
- Oyonarte, C., Perez-Pujalte, A., Delgado, G., Delgado, R., & Almendros, G. (1994). Factors affecting soil organic-matter turnover in a Mediterranean ecosystem from Sierra de Gádor (Spain) – an analytical approach. *Communications in Soil Science and Plant Analysis*, 25, 1929–1945.
- Oyonarte, C., Escoriza, I., Delgado, R., Pinto, V., & Delgado, G. (1998). Water-retention capacity in fine earth and gravel fractions of semiarid Mediterranean montane soils. *Arid Soil Research and Rehabilitation*, 12(1), 29–45.
- Paracuellos, M. (2006). How can habitat selection affect the use of a wetland complex by waterbirds? *Biodiversity and Conservation*, 15, 4569–4582.
- Paruelo, J. M., Sala, O. E., & Beltran, A. B. (2000). Long-term dynamics of water and carbon in semi-arid ecosystems: a gradient analysis in the Patagonian steppe. *Plant Ecology*, 150, 133–143.
- Perez de Perceval, M. A. (1984). *Fundidores, mineros y comerciantes: la metalurgia de Sierra de Gádor 1820–1850*. Almería: Cajamar.
- Phillips, J. D. (1993). Biophysical feedbacks and the risks of desertification. *Annals of the Association of American Geographers*, 83, 630–640.
- Potter, C., Tan, P. N., Steinbach, M., Klooster, S., Kumar, V., Myneni, R., et al. (2003). Major disturbance events in terrestrial ecosystems detected using global satellite data sets. *Global Change Biology*, 9, 1005–1021.
- Poyatos, R., Llorens, P., & Gallart, F. (2005). Transpiration of montane *Pinus sylvestris* L. and *Quercus pubescens* Willd. forest stands measured with sap flow sensors in NE Spain. *Hydrology and Earth System Sciences*, 9, 493–595.
- Prihodko, L., & Goward, S. N. (1997). Estimation of air temperature from remotely sensed surface observations. *Remote Sensing of Environment*, 60, 335–346.
- Prince, S. D., De Colstoun, E. B., & Kravitz, L. L. (1998). Evidence from rain-use efficiencies does not indicate extensive Sahelian desertification. *Global Change Biology*, 4, 359–374.
- Pugnaire, F. I., Haase, P., Puigdefábregas, J., Cueto, M., Clark, S. C., & Incoll, L. D. (1996). Facilitation and succession under the canopy of a leguminous shrub, *Retama sphaerocarpa*, in a semi-arid environment in south-east Spain. *Oikos*, 76, 455–464.
- Puigdefábregas, J., Delgado, L., Domingo, F., Cueto, M., Gutiérrez, L., Lázaro, R., et al. (1996). The Rambla Honda field site: interactions of soil and vegetation along a catena in semi-arid southeast Spain. In J. Brandt, & J. Thornes (Eds.), *Mediterranean Desertification and Land Use* (pp. 137–168). John Wiley & Sons, Ltd.
- Puigdefábregas, J. (1995). Desertification – stress beyond resilience, exploring a unifying process structure. *Ambio*, 24, 311–313.
- Puigdefábregas, J. (1998). Ecological impacts of global change on drylands and their implications for desertification. *Land Degradation & Development*, 9, 393–406.
- Puigdefábregas, J. (2005). The role of vegetation patterns in structuring runoff and sediment fluxes in drylands. *Earth Surface Processes and Landforms*, 30, 133–147.
- Puigdefábregas, J., & Mendizabal, T. (1998). Perspectives on desertification: western Mediterranean. *Journal of Arid Environments*, 39, 209–224.
- Puigdefábregas, J., Sole, A., Gutierrez, L., del Barrio, G., & Boer, M. (1999). Scales and processes of water and sediment redistribution in drylands: results from the Rambla Honda field site in Southeast Spain. *Earth-Science Reviews*, 48, 39–70.
- Pulido-Bosch, A., Pulido-Leboeuf, P., Molina-Sanchez, L., Vallejos, A., & Martin-Rosales, W. (2000). Intensive agriculture, wetlands, quarries and water management. A case study (Campo de Dalías, SE Spain). *Environmental Geology*, 40, 163–168.
- Reynolds, J. F., Smith, D. M. S., Lambin, E. F., Turner, B. L., Mortimore, M., Batterbury, S. P. J., et al. (2007). Global desertification: building a science for dryland development. *Science*, 316, 847–851.
- Roerink, G. J., Su, Z., & Menenti, M. (2000). S-SEBI: a simple remote sensing algorithm to estimate the surface energy balance. *Physics and Chemistry of the Earth Part B-Hydrology Oceans and Atmosphere*, 25, 147–157.
- Safriel, U., Adeel, Z., Niemeijer, D., Puigdefábregas, J., White, R., Lal, R., et al. (2003). Dryland systems. *Ecosystems & human well-being. Current state and trends Millennium Ecosystem Assessment Series*. (pp. 623–662) Washington, DC: World Resources Institute.
- Samani, Z., Bawazir, A. S., Bleiweiss, M., Skaggs, M., & Vien, D. (2007). Estimating daily net radiation over vegetation canopy through remote sensing and climatic data. *Journal of Irrigation and Drainage Engineering*, 133(4), 291–297.
- Schlesinger, W. H., Reynolds, J. F., Cunningham, G. L., Huenneke, L. F., Jarrell, W. M., Virginia, R. A., et al. (1990). Biological feedbacks in global desertification. *Science*, 247, 1043–1048.
- Seguin, B., Becker, F., Pulpin, T., Gu, X. F., Guyot, G., Kerr, Y., et al. (1999). IRSUTE: a minisatellite project for land surface heat flux estimation from field to regional scale. *Remote Sensing of Environment*, 68, 357–369.
- Seguin, B., & Itier, B. (1983). Using midday surface-temperature to estimate daily evaporation from satellite thermal IR data. *International Journal of Remote Sensing*, 4, 371–383.
- Sharma, K. D. (1998). The hydrological indicators of desertification. *Journal of Arid Environments*, 39, 121–132.
- Shuttleworth, W. J., & Wallace, J. S. (1985). Evaporation from sparse crops – an energy combination theory. *Quarterly Journal of the Royal Meteorological Society*, 111, 839–855.
- Sobrinho, J. A., & Raissouni, N. (2000). Toward remote sensing methods for land cover dynamic monitoring: application to Morocco. *International Journal of Remote Sensing*, 21, 353–366.
- Soil Survey Staff (1990). Keys to soil taxonomy. *SMSS Technical Monograph, N° 19*, 422. (pp. )Blacksburg, VA: Virginia Polytechnic and State University.
- StatSoft, Inc. (2005). *STATISTICA (data analysis software system), version 7.1*. [www.statsoft.com](http://www.statsoft.com)
- Stolt, M. H., & Baker, J. C. (1994). Strategies for studying saprolite and saprolite genesis. In D. L. Cremeens, R. B. Brown, & J. H. Huddleston (Eds.), *Whole regolith pedology* (pp. 1–19). SSSA Special Publication.
- Su, Z. (2002). The Surface Energy Balance System (SEBS) for estimation of turbulent heat fluxes. *Hydrology and Earth System Sciences*, 6, 85–99.
- Sugita, M., & Brutsaert, W. (1991). Daily evaporation over a region from lower boundary-layer profiles measured with radiosondes. *Water Resources Research*, 27, 747–752.
- Villagarcía, L., Were, A., Domingo, F., García, M., & Alados-Arboledas, L. (2007). Estimation of soil boundary-layer resistance in sparse semiarid stands for evapotranspiration modelling. *Journal of Hydrology*, 342, 173–183.
- Timmermans, W. J., Kustas, W. P., Anderson, M. C., & French, A. N. (2007). An intercomparison of the surface energy balance algorithm for land (SEBAL) and the two-source energy balance (TSEB) modeling schemes. *Remote Sensing of Environment*, 108, 369–384.
- Tucker, C. J., & Nicholson, S. E. (1999). Variations in the size of the Sahara Desert from 1980 to 1997. *Ambio*, 28, 587–591.
- UNCCD (1996). United Nations Convention to Combat Desertification in Those Countries Experiencing Serious Drought and/or Desertification, Particularly in Africa. U.N. Doc., A/AC.241/27; 71.
- Valle, F. (2003). Mapa de Series de Vegetación de Andalucía. Editorial Rueda. Sevilla 131 pp.
- Vandegriend, A. A., & Owe, M. (1993). On the relationship between thermal emissivity and the normalized difference vegetation index for natural surfaces. *International Journal of Remote Sensing*, 14, 1119–1131.
- Vanderlinden, K., Giraldez, J. V., & Van Meirvenne, M. (2004). Assessing reference evapotranspiration by the Hargreaves method in southern Spain. *Journal of Irrigation and Drainage Engineering*, 130, 184–191.

- Verstraeten, W. W., Veroustraete, F., & Feyen, J. (2005). Estimating evapotranspiration of European forests from NOAA-imagery at satellite overpass time: towards an operational processing chain for integrated optical and thermal sensor data products. *Remote Sensing of Environment*, 96, 256–276.
- Vidal, S., 1994. Sensor para la determinación simultánea en suelos de humedad y conductividad eléctrica. Patent no. 9401681.
- Villagarcía, L., Domingo, F., Alados-Arboledas, L., & Puigdefábregas, J. (2001). Modelización de la evapotranspiración real en rodales de tres especies vegetales del SE español. V Simposio sobre el agua en Andalucía. Editorial de la Universidad de Almería, Almería, 1. (pp. 107–118).
- Wang, Q. X., & Takahashi, H. (1998). Regional hydrological effects of grassland degradation in the Loess Plateau of China. *Hydrological Processes*, 12, 2279–2288.
- Wassenaar, T., Olioso, A., Hasager, C., Jacob, F., & Chehbouni, A. (2002). J.A. Estimation of evapotranspiration on heterogeneous pixels. In J. A. Sobrino (Ed.), *Recent Advances in Quantitative Remote Sensing* (pp. 458–465). Universidad de Valencia 84–370-5515-6.
- Were, A., Villagarcía, L., Domingo, F., Alados-Arboledas, L., & Puigdefábregas, J. (2007). Analysis of effective resistance calculation methods and their effect on modelling evapotranspiration in two different patches of vegetation in semi-arid SE Spain. *HESSD (Hydrology and Earth System Sciences Discussions)*, 4, 1–44.
- Wessels, K. J., Prince, S. D., Frost, P. E., & van Zyl, D. (2004). Assessing the effects of human-induced land degradation in the former homelands of northern South Africa with a 1 km AVHRR NDVI time-series. *Remote Sensing of Environment*, 91, 47–67.
- Wilson, K. B., Baldocchi, D. D., Aubinet, M., Berbigier, P., Bernhofer, C., Dolman, H., et al. (2002). Energy partitioning between latent and sensible heat flux during the warm season at FLUXNET sites. *Water Resources Research*, 38 30–1/30–11.
- Xue, Y. K., & Shukla, J. (1993). The influence of land-surface properties on Sahel climate 1. Desertification. *Journal of Climate*, 6, 2232–2245.